AlphaFold Database Debiasing for Robust Inverse Folding

Cheng Tan[1*] **Zhenxiao Cao**[2*] **Zhangyang Gao**[1*] **Siyuan Li**[3] **Yufei Huang**[3] **Stan Z. Li**[3]
[1]Shanghai AI Laboratory [2]Hong Kong University of Science and Technology
[3]AI Lab, Research Center for Industries of the Future, Westlake University

Abstract

The AlphaFold Protein Structure Database (AFDB) offers unparalleled structural coverage at near-experimental accuracy, positioning it as a valuable resource for data-driven protein design. However, its direct use in training deep models that are sensitive to fine-grained atomic geometry—such as inverse folding—exposes a critical limitation. Comparative analysis of structural feature distributions reveals that AFDB structures exhibit distinct statistical regularities, reflecting a systematic geometric bias that deviates from the conformational diversity found in experimentally determined structures from the Protein Data Bank (PDB). While AFDB structures are cleaner and more idealized, PDB structures capture the intrinsic variability and physical realism essential for generalization in downstream tasks. To address this discrepancy, we introduce a **De**biasing **S**tructure **A**uto**E**ncoder (DeSAE) that learns to reconstruct native-like conformations from intentionally corrupted backbone geometries. By training the model to recover plausible structural states, DeSAE implicitly captures a more robust and natural structural manifold. At inference, applying DeSAE to AFDB structures produces debiased representations that significantly improve inverse folding performance across multiple benchmarks, and also enhance other structure-conditioned modeling tasks. This work highlights the critical impact of subtle systematic biases in predicted structures and presents a principled framework for debiasing, significantly boosting the performance of structure-based learning tasks like inverse folding.

1 Introduction

The advent of highly accurate protein structure prediction, epitomized by AlphaFold2 [1, 2, 3], has fundamentally reshaped the landscape of molecular biology. The resulting AlphaFold Protein Structure Database (AFDB) [4, 5, 6] provides an unprecedented repository of structural information, covering vast swathes of the known proteome with near-experimental resolution. This deluge of data promises to catalyze breakthroughs in data-driven protein analysis and design, offering fertile ground for deep learning models to decipher the complex sequence-structure-function relationship. Yet, despite their accuracy, AlphaFold-predicted structures differ systematically from experimentally determined ones. These differences reflect the inductive biases of the predictive model itself—biases which, although benign for folding, can impair downstream learning tasks.

The challenge posed by this systematic bias becomes particularly salient in applications demanding high structural fidelity, such as inverse folding—the prediction of amino acid sequences compatible with a given protein backbone. This task is exquisitely sensitive to the precise geometric and energetic details of the target structure. To empirically demonstrate this, we investigated the performance of several representative inverse folding models when trained on different structural datasets and on a consistent, held-out set of experimentally determined PDB structures.

[*]Equal contribution.

Specifically, models such as StructGNN [7], GraphTrans [7], GVP [8], and PiFold [9] were trained independently: once using a curated dataset of high-quality PDB structures, and again using a comparable dataset of high fidelity (pLDDT $>$ 70) AFDB structures. Despite the close structural agreement between the two datasets—as indicated by an average RMSD of approximately 0.2Å(Figure 1a)—the downstream performance on the inverse folding task diverged sharply. As shown in Figure 1(b), models trained on PDB data achieved recovery rates between 34.11% and 43.76%, while those trained on AFDB structures performed markedly worse, with recovery rates ranging from 17.16% to 27.83%. The most extreme degradation was observed for PiFold, which dropped from 43.76% to 17.16% when trained on AFDB data. Intriguingly, we observed a consistent trend: models that performed better on PDB data suffered more acutely when trained on AFDB data—suggesting that stronger models are more prone to overfitting the subtle, non-physical regularities present in AFDB data.

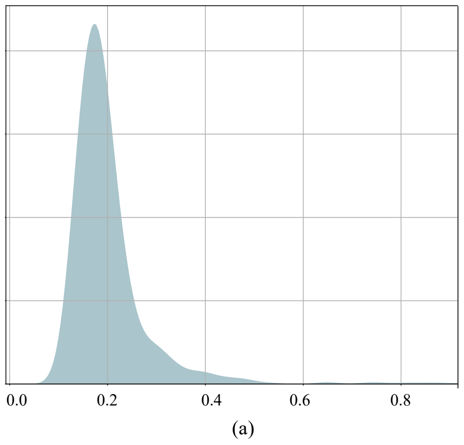

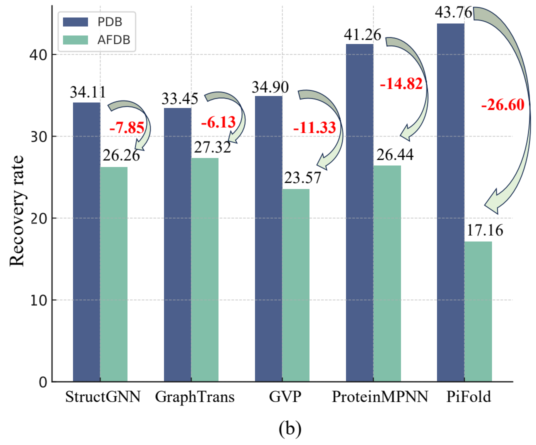

Figure 1: (a) The RMSD distribution of paired structure data from AFDB and PDB. (b) Recovery rate of representative inverse folding methods trained on PDB and AFDB.

These findings provide direct evidence of a distributional shift between AlphaFold-predicted and experimentally observed structures. This performance gap reveals a tangible cost of structural bias: although AFDB structures are highly confident from the model's perspective, they inhabit a displaced region of conformational space—more geometrically idealized, less variable, and ultimately less reflective of the structural diversity sampled in nature. As a result, models trained exclusively on AFDB data fail to generalize reliably to real-world proteins, underscoring the importance of structural realism in downstream design tasks and highlighting the need for principled debiasing strategies.

To intuitively illustrate the divergence between predicted and experimentally determined protein structures, we analyze the distribution of fundamental structural features—such as dihedral angles and inter-atomic distances—across AFDB and PDB. While AFDB structures are generally accurate at the fold level, they tend to occupy a smoother, more regularized region of conformational space—reflecting the inductive biases of the AlphaFold. To bridge this gap and align AFDB structures more closely with experimentally validated conformations, we introduce the Debiasing Structure Autoencoder (DeSAE), a framework trained to reconstruct plausible native conformations from deliberately corrupted backbone geometries. DeSAE learns the structural manifold of experimentally observed proteins, effectively debiasing synthetic structures and improving their downstream utility.

Our main contributions are as follows:

- **Systematic Characterization of Predictive Bias:** We provide, to our knowledge, the first comprehensive identification and quantification of systematic statistical deviations in AFDB when compared against the ensemble of experimental PDB structures.
- **A Debiasing Framework via Manifold Learning:** We introduce DeSAE, a principled framework that learns the manifold of experimentally plausible protein conformations. By training on a denoising objective, DeSAE learns to project AFDB structures onto more realistic structural space.
- **Enhanced Generalization for Inverse Folding:** We rigorously demonstrate that training inverse folding models on DeSAE-debiased AFDB structures leads to consistent and statistically significant improvements in generalization performance across multiple standard benchmarks, validating the practical utility of our debiasing approach.

2 Related Work

2.1 AlphaFold Database and Its Applications

The development of AlphaFold2 [1] and its subsequent expansion into the AFDB [4] represents a monumental leap in structural biology [10, 11, 12]. AFDB provides open access to millions of high-accuracy predicted protein structures, drastically expanding the known structural proteome far beyond what has been experimentally determined via methods like X-ray crystallography, NMR, or cryo-EM deposited in the PDB [13]. This unprecedented resource has rapidly become foundational for a plethora of applications. Researchers have leveraged AFDB for large-scale functional annotation [14, 15, 16], understanding protein-protein interactions [2, 17], identifying novel drug targets [18, 19], and accelerating structural analysis of complex biological systems [20, 21]. Indeed, structure prediction models like AlphaFold3 [3] have reportedly incorporated AlphaFold2-predicted structures into their training regimens, albeit often with mixed strategies incorporating experimental data.

2.2 Structure-based Inverse Folding

Inverse protein folding [22, 23, 24, 25]—the task of predicting an amino acid sequence that will fold into a given three-dimensional backbone structure—is a foundational problem in computational protein design [26, 27, 28, 29, 30]. Historically, this problem was approached using physics-based energy functions [31], but recent advances in deep learning have enabled substantial improvements in both accuracy and scalability [32, 33, 34]. Early methods employed multilayer perceptrons (MLPs) to estimate the probability distribution over 20 amino acids for each residue, based on structural features [35, 36, 37, 38, 39, 40, 41]. Graph-based methods further extend this framework by modeling the protein as a k-nearest neighbor graph [42, 43, 44]. StrutGNN and GraphTrans [7] introduced a graph encoder coupled with an autoregressive decoder. GVP [8] leveraged geometric vector perceptrons to jointly learn scalar and geometric vector features. GCA [45] employed global attention mechanisms to capture long-range dependencies. ProteinSolver [46] have addressed partially known sequences, while models like AlphaDesign [47], ProteinMPNN [48], and ESM-IF [49] have achieved strong performance by training on large structural datasets. Several recent works [50, 51] introduce protein language models [52, 53, 54, 55] or surface-based representations [56, 57] to improve inverse folding. Furthermore, many structure-based tasks [58, 59, 60, 61, 62], such as predicting ligand binding sites [63, 64, 65, 66], enzyme commission numbers [67, 68, 69, 70, 71, 72], protein-protein interaction interfaces [73, 74, 75], or post-translational modification [76, 77], also critically depend on precise tertiary structure, often using representations learned by inverse folding models or similar geometric deep learning architectures. Therefore, the fidelity of the structural data used for training these models is paramount. The systematic biases we identify in AFDB could propagate and amplify in such highly sensitive protein structure-based applications, motivating our development of a structural debiasing framework to improve robustness and accuracy of these downstream tasks.

3 Preliminaries

A protein can be represented as a sequence of amino acids $S^L = (s_1, s_2, ..., s_L)$ of length L, where $s_i \in \mathcal{A}$ and $\mathcal{A}$ denotes the standard amino acid alphabet. The corresponding 3D structure of the protein is defined by the Cartesian coordinates of its backbone atoms—typically including the nitrogen (N), alpha carbon (C$_\alpha$), and carbon (C) atoms for each residue. We denote the backbone conformation as $X^L = \{\boldsymbol{x}_{i,a} \in \mathbb{R}^3 \mid i = 1, \dots, L; a \in \mathcal{B}\}, \mathcal{B}_i = \{\mathrm{N}, \mathrm{C}\alpha, \mathrm{C}, \mathrm{O}\}$.

Protein Structure Prediction refers to the task of inferring the 3D structure X from the amino acid sequence S. This is typically formulated as learning a function $f : S^L \to X^L$, where the model predicts the atomic coordinates that define the protein's conformation. AlphaFold2 [1], as a notable example, approximates it with remarkable accuracy, making it a cornerstone of structural biology.

Inverse Folding, also known as structure-based sequence design, is the complementary problem. Given a target backbone conformation X, the goal is to recover a sequence S that is likely to fold into X. This task can be expressed probabilistically as modeling the conditional distribution $p(S \mid X)$, or deterministically as learning a function $g : X^L \to S^L$.

As illustrated in Figure 2, inverse folding relies on structure-to-sequence reasoning, in contrast to the sequence-to-structure of prediction models like AlphaFold2. Crucially, this directional shift makes inverse folding models vulnerable to distributional artifacts in the structural data they are trained on.

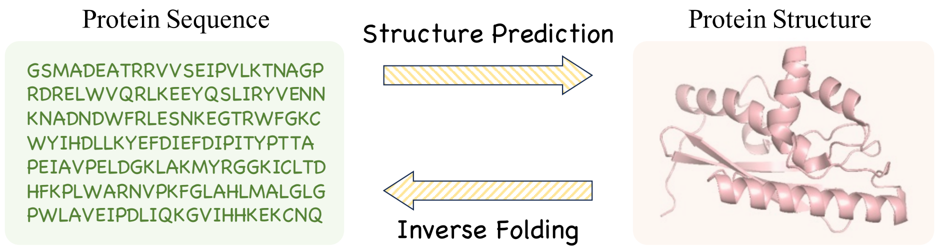

Figure 2: Conceptual comparison between protein structure prediction (sequence-to-structure) and inverse folding (structure-to-sequence).

Why Inverse Folding Reveals Structural Bias? We adopt inverse folding as the primary lens through which to study bias in predicted structures. Unlike structure prediction—where small geometric inaccuracies may be tolerable—inverse folding requires a high-fidelity representation of the structural manifold. Any systematic bias in the input structure distribution can distort the learned mapping from structure to sequence. Learning the conditional distribution $p(S|X)$ requires the model to capture fine-grained and context-specific geometric feature.

The Structural Debiasing Task The core challenge motivating this work stems from the observation that while models trained on predicted structures X_{pred} (e.g., from AFDB) may perform well on similar held-out predicted data, their generalization to experimental data X_{exp} (e.g. from PDB) can be suboptimal. We define the structural debiasing task as learning a transformation $\mathcal{T}$ that debias X_{pred} into a structure $X'_{\text{pred}} = \mathcal{T}(X_{\text{pred}})$. The primary objective is not merely to alter X_{pred}, but to ensure that downstream models trained or evaluated using X'_{pred} exhibit improved generalization.

In the specific context of inverse folding, let $\mathcal{F}$ denote an inverse folding model trained on a dataset of structures. When $\mathcal{F}$ is trained on debiased structures $X'\text{pred}$, its effectiveness is evaluated based on its ability to recover amino acid sequences for a held-out set of experimental structures $X\text{exp}$. Let $M(\cdot)$ be a performance metric for the downstream task—e.g., the sequence recovery rate. The transformation $\mathcal{T}$ is considered beneficial if it satisfies the following condition:

$$M(\mathcal{F}(X'_{\text{pred}})) > M(\mathcal{F}(X_{\text{pred}})) \tag{1}$$

with the ideal objective being to approach:

$$M(\mathcal{F}(X'_{\text{pred}})) \to M(\mathcal{F}(X_{\text{exp}})) \tag{2}$$

That is, the model trained on debiased predicted structures should generalize as well as, or nearly as well as, a model trained on high-quality experimental structures.

4 Uncovering Systematic Structural Bias in AFDB

4.1 Manifestation of Bias: Degraded Performance in Inverse Folding

To empirically evaluate the impact of training exclusively on predicted structures, we constructed a rigorously curated dataset of paired PDB and AFDB entries (see Appendix B.1). We adopt the validation and test splits from CATH 4.2 [78], removing any entries with high sequence similarity with our paired dataset. It is important to note that only the training partition is altered. As previously shown in Figure 1, although the predicted AFDB structures exhibit close agreement with experimental structures, the inverse folding performance of models trained on AFDB structures is markedly worse than those trained on PDB data. This phenomenon is further elucidated by examining the learning dynamics when trained and validated across PDB and AFDB data, as depicted in Figure 3. While models trained on either PDB or AFDB data exhibit superficially similar decreases in training loss (Figures 3a and 3c), a stark divergence emerges in their validation performance. Notably, models trained on AFDB data demonstrate a pronounced difficulty in generalizing, as evidenced by significantly higher or more erratic validation losses on held-out PDB structures (Figure 3d) compared to the robust generalization observed when training and validating on PDB data (Figure 3b).

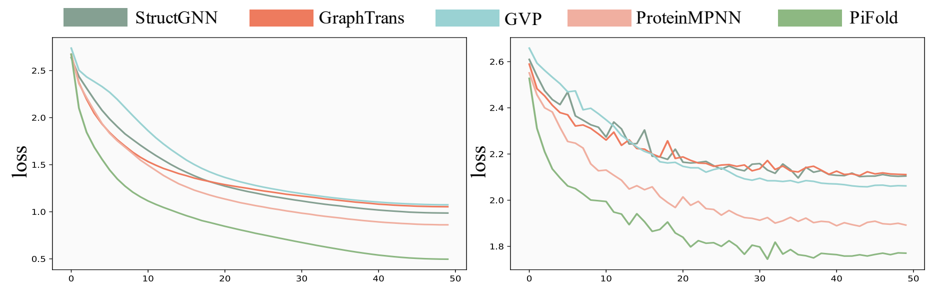

(a) Training loss curve trained on PDB (b) Validation loss curve trained on PDB

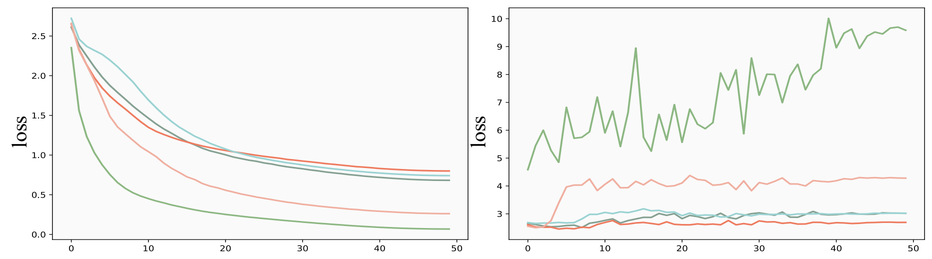

(c) Training loss curve trained on AFDB (d) Validation loss curve trained on AFDB

Figure 3: Training and validation loss curves for inverse folding models on PDB and AFDB datasets.

4.2 Statistical Analysis of Key Structure Features

We performed a comparative statistical analysis of fundamental structural features. We focused on dihedral angles ϕ, ψ, ω and bond lengths (C-Cα and N-Cα) in the main text, as these parameters critically define local protein conformation. More detailed analysis is provided in Appendix E.

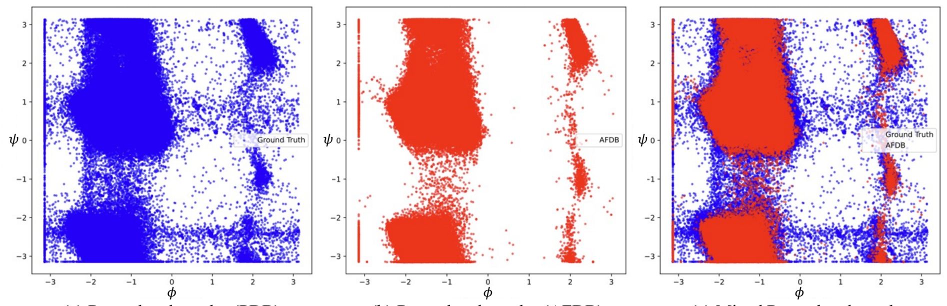

(a) Ramachandran plot (PDB) (b) Ramachandran plot (AFDB) (c) Mixed Ramachandran plot

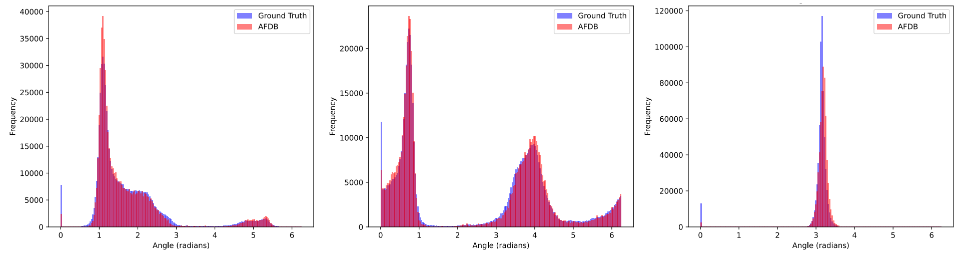

(d) ϕ distribution comparison (e) ψ distribution comparison (f) ω distribution comparison

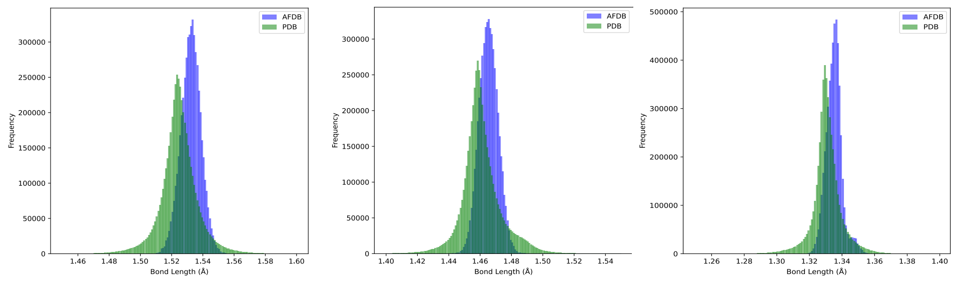

(g) C-Cα distance Comparison (h) N-Cα distance Comparison (i) C-N distance Comparison

Figure 4: Statistical comparison of key structural features between paired PDB and AFDB data.

The Ramachandran plot for PDB (Figure 4a) displays well-defined clusters corresponding to canonical secondary structures (α-helices, β-sheets), but also a significant dispersion of points into less populated and even classically "disallowed" regions. In stark contrast, AFDB structures (Figure 4b) shows considerably tighter, more concentrated clusters within the allowed regions, with a notably sparser population in the disallowed areas. The mixed plot (Figure 4c) vividly demonstrates this: AFDB conformations predominantly occupy the core of the allowed regions, while PDB conformations form a broader envelope and populate peripheral regions more extensively.

Direct comparison of the ϕ, ψ, and ω dihedral angle distributions further substantiates these observations. For both ϕ and ψ angles, the AFDB distributions exhibit sharper, higher peaks and narrower spreads compared to the PDB distributions. The ω angle distribution, predominantly centered around π radians, also shows a more constrained, needle-like peak for AFDB compared to the slightly broader peak observed for PDB, which can accommodate subtle deviations and cis-peptide bonds. Analysis of backbone bond lengths reinforces this trend of reduced variability in AFDB. The PDB bond length distributions exhibit broader tails, indicative of a greater range of bond distortions reflecting real physical variations or experimental factors.

5 Method

The observed "idealization" or regularization bias within AFDB data leads to a narrower distribution of local geometric parameters compared to experimental data. This discrepancy can hinder the development of robust deep learning models for tasks that critically depend on precise atomic details. To address this issue, we propose a simple yet effective **Debiasing Structure Autoencoder (DeSAE)**, illustrated in Figure 5. DeSAE is designed to reconstruct native-like conformations from biased or corrupted structural inputs, thereby learning a generalizable structural manifold.

Structure Corruption Strategy We introduce localized perturbations to the backbone coordinates. Specifically, we randomly select a subset of residues and choose one of their backbone atoms. The coordinates of the chosen atom a^* is replaced by the centroid of the remaining three atoms:

$$x'_{i,a^*} = 1/3 \sum_{a \in \mathcal{B}_i \setminus \{a^*\}} x_{i,a}, \tag{3}$$

This strategy forces the model to learn local geometric integrity based on contextual information from the rest of the structure, using the uncorrupted PDB structure as the ground truth for reconstruction.

DeSAE Architecture In DeSAE, each residue i is associated with a local frame $T_i(R_i, t_i)$, where $R_i \in \mathrm{SO}(3)$ is a rotation matrix and $t_i \in \mathbb{R}^3$ is a translation vector (typically centered at Cα). Node features are denoted $h_i \in \mathbb{R}^D$ and edge features between node s and t are $h_{ij} \in \mathbb{R}^D$. In the SE(3) encoder, we employ only the *frame aggregation* layers to capture local geometric interactions. In contrast, the SE(3) decoder utilizes both *frame aggregation* and *frame update* layers, allowing the model to iteratively refine local frames and recover physically consistent backbone geometries.

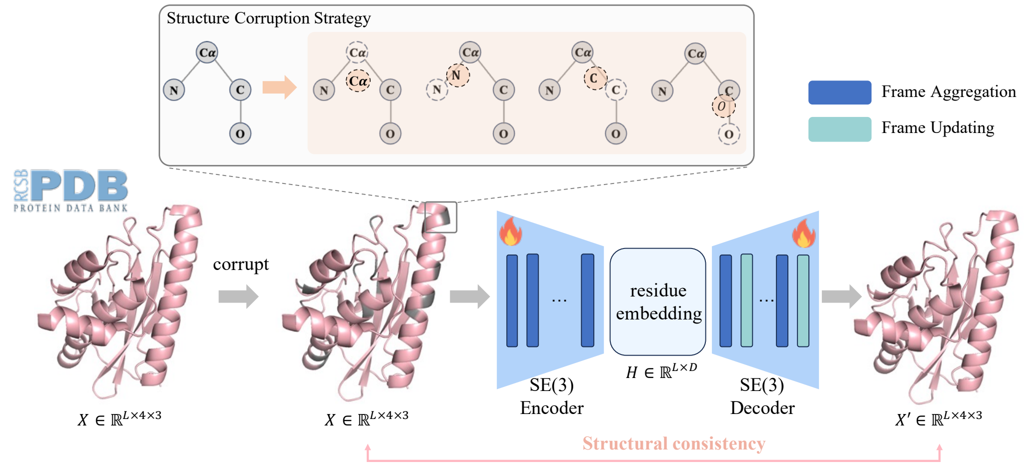
Structure Corruption Strategy
Cα
N
C
O
Frame Aggregation
Frame Updating
corrupt
residue embedding
$H \in \mathbb{R}^{L\times D}$
SE(3) Encoder
SE(3) Decoder
$X \in \mathbb{R}^{L\times 4\times 3}$
$X \in \mathbb{R}^{L\times 4\times 3}$
$X' \in \mathbb{R}^{L\times 4\times 3}$
Structural consistency

Figure 5: Overview of the DeSAE. The encoder utilizes Frame Aggregation layers to build informative residue and edge representations invariant to global pose. The decoder employs both Frame Aggregation/Updating layers to refine residue frames and reconstruct the debiased protein structure.

Frame Aggregation This module updates node and edge embeddings by processing information in a manner invariant to global rigid transformations. For a pair of nodes (i, j) and their respective frames T_i, T_j at layer l, the update process can be summarized as:

$$h_{ij}^{(l+1)}, h_i^{(l+1)} = \text{FrameAgg}(h_{ij}^{(l)}, h_i^{(l)}, T_i, T_j), \tag{4}$$

The aggregation involves several steps:

1. **Projection to latent geometric space**: Node and edge features are projected into a latent 3D space, yielding sets of "virtual atom" coordinates associated with each node and edge:
$$z_i^{(l)} = \mathcal{Z}_\theta(h_i^{(l)}), z_{ij}^{(l)} = \mathcal{Z}_\theta(h_{ij}^{(l)}), \tag{5}$$
where $\mathcal{Z}_\theta(\cdot) : \mathbb{R}^D \to \mathbb{R}^{m\times 3}$ is a learnable function typically parameterized by MLP followed by reshaping, m represents the number of virtual points.
2. **Augmented edge embedding with relative frame geometry**: To incorporate geometric context, the edge feature is augmented using the relative pose between local frames. The relative transformation is given by $T_{ij} = T_i^{-1} \circ T_j$, and applied to the edge projection:
$$p_{ij} = (T_{ij} \circ z_{ij}^{(l)})||z_{ij}^{(l)}, \tag{6}$$
3. **Inter-node geometric interaction**: To capture the geometric relationship between the nodes themselves, their latent point clouds $z_i^{(l)}$ and $z_j^{(l)}$ are compared after aligning them within a common reference frame, typically frame i. The points $z_j^{(l)}$ are transformed using the relative rotation $R_i^T R_j$ before calculating the geometric dot product with $z_i^{(l)}$.
$$q_{ij} = z_i^{(l)}(R_i^T R_j z_j^{(l)})^T, \tag{7}$$
4. **Edge aggregating**: The final edge embedding $h_{ij}^{(l+1)}$ is aggregated by integrating the augmented geometric features ($p_{ij}^{(l)}$, $q_{ij}^{(l)}$) and explicit relative frame information:
$$h_{ij}^{(l+1)} = \text{MLP}(p_{ij}, q_{ij}, \text{vec}(R_{ij}), \|t_s - t_t\|), \tag{8}$$
5. **Node aggregating**: The node embedding is aggregated by weighted neighboring nodes:
$$h_i^{(l+1)} = \text{MLP}(h_i^{(l)} + \sum_{j\in\mathcal{N}_i} a_{ij} h_j^{(l+1)}), \tag{9}$$
where $\mathcal{N}_i$ denotes the set of neighboring nodes, and a_{ij} is the attention weight.

Frame Updating The Frame Updating module, employed exclusively within the decoder, is responsible for refining the residue-specific local frames $T_i^{(l)} = (R_i^{(l)}, t_i^{(l)})$ at layer l to produce updated frames $T_i^{(l+1)} = (R_i^{(l+1)}, t_i^{(l+1)})$ for the subsequent layer.

1. **Rotation updating**: The updated rotation $R_i^{(l)}$ is predicted based on an attention-weighted aggregation of the relative orientations of neighboring frames:
$$\begin{aligned} \text{vec}(R_i^{(l)}) &= \sum_{j\in\mathcal{N}_i} a_{ij}^r \text{vec}(R_{ij}^{(l)}), \\ R_i^{(l+1)} &= \text{Quat2Rot}(W_r \text{vec}(R_i^{(l)})), \end{aligned} \tag{10}$$
where a_{ij}^r is the learnable attention weight, $W_r \in \mathbb{R}^{4\times 9}$ projects the vectorized matrix into the 4D space. $\text{Quat2Rot}(\cdot)$ maps a quaternion to its corresponding 3×3 rotation matrix, detailed in Appendix A.2.
2. **Translation updating**: The updated translation $t_i^{(l+1)}$ is determined by an attention-weighted aggregation of relative positional information derived from neighboring residues:
$$t_i^{(l+1)} = \sum_{j\in\mathcal{N}_i} a_{ij}^t t_{ij}^{(l)}, \tag{11}$$
where a_{ij}^t is the learnable attention weight. The coordinates are determined by $x_i = T_i^{(l)} \circ h_i$.

Structural consistency We employ the structure loss inspired by Chroma [79], which aims to directly minimize the deviation between the predicted and reference backbone conformations. The detailed loss function is provided in the Appendix A.1.

6 Experiments

We begin by curating a paired dataset of experimentally determined structures from PDB and their corresponding AFDB data (see Appendix B). We first pretrain DeSAE with the proposed structure corruption strategy that corrupt randomly 10% residues. The trained DeSAE was then applied to the AFDB structures to produce a "Debiased AFDB" dataset. **Due to its simple design, DeSAE has only 5.9M parameters and is capable of processing process about 20k AFDB structures in 3 minutes on a single NVIDIA A100 GPU.** To assess the impact of this debiasing, we evaluated these datasets on a downstream inverse folding task. Specifically, the inverse folding model was trained independently using three distinct datasets: (1) PDB, (2) AFDB, and (3) Debiased AFDB. Further specifics on model architectures, and experimental parameters are provided in Appendix C.

6.1 Does Debiasing Work?

We train models on three datasets and evaluate them using the validation and test sets of CATH 4.2 [78]. A critical aspect of structural debiasing is the preservation of the overall protein fold. Figure 6(a) presents the RMSD distribution remain concentrated at low values, and even seems unchanged compared to Figure 1(a), indicating that the debiasing process effectively debias AFDB without introducing significant global distortions. More importantly, the Debiased AFDB enables substantial improvements in sequence recovery across five inverse folding models (Figure 6(b)).

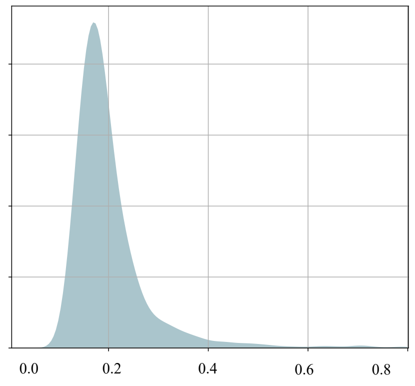

(a)

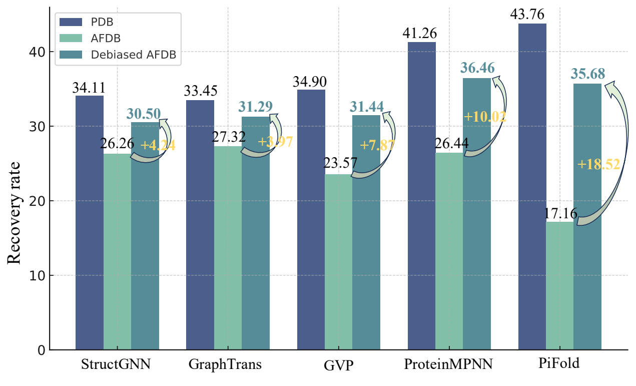

(b)

Figure 6: (a) The RMSD distribution of paired structure data from Debiased AFDB and PDB. (b) Recovery rate of inverse folding methods trained on three datasets and evaluated on CATH 4.2.

Training dynamics on the Debiased AFDB are more favorable than on the original AFDB. As depicted in Figure 7, the validation loss exhibits a decay thrend over training epochs. While it remains less stable than training on PDB, it is significantly more stable and lower in magnitude than that observed for AFDB-trained models (see Figure 3). These results collectively affirm that our DSAE not only preserves structural accuracy but also enhances the learnability of inverse folding models.

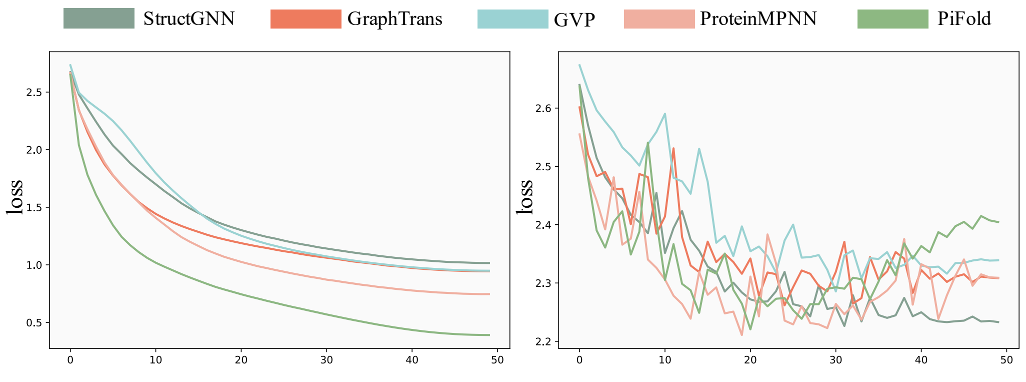

(a) Training loss curve trained on PDB (b) Validation loss curve trained on PDB

Figure 7: Training and validation loss curves for inverse folding models on Debiased AFDB.

6.2 Does Debiasing Generalizable?

To assess the generalization capability of our Debiased AFDB, we use the trained model further evaluate on TS50 and TS500 test sets, which represent diverse and difficult inverse folding challenges. As shown in Figure 8, the performance advantages of Debiased AFDB persist on both TS50 and TS500 benchmarks. Similarly, results on the CATH 4.3 test set reproted Table 1 reinforce this trend. Across all five inverse folding models training on Debiased AFDB leads to consistent improvements in sequence recovery compared to training on original AFDB structures. These results strongly indicate that our debiasing methodology effectively enhances the structural realism of AFDB data, enabling models to learn more generalizable sequence-structure relationships.

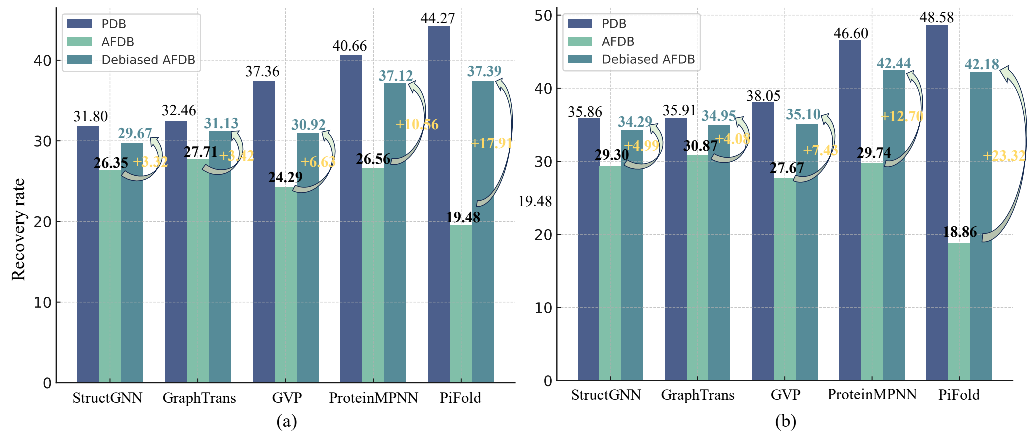

Figure 8: Recovery rate of inverse folding methods trained on PDB, AFDB, and Debiased AFDB. (a) Test on TS50 benchmark. (b) Test on TS500 benchmark.

6.3 Does Larger Scale Pretraining DeSAE Benefit Downstream Task?

The default DeSAE model is pretrained on the PDB subset of our paired dataset, which comprises approximately 20,000 structures. To explore the benefits of larger-scale pretraining, we further pretrain DeSAE on the full PDB dataset and apply our debiasing pipeline to the AFDB data of the paired dataset. We refer to this extended dataset as Debiased AFDB-XL. As shown in Table 1, Debiased AFDB-XL yields modest improvements over the Debiased AFDB. However, the overall gains are limited. A possible reason is that DeSAE primarily captures local geometric features, and thus may not fully benefit from additional global or large-scale structural diversity in pretraining.

Table 1: Recovery rate (%) of inverse folding methods trained on different data and test on the CATH 4.3 test set. The footnote colored in blue indicates the improvement of Debiased AFDB over the AFDB, colored in green indicates the improvement of Debiased AFDB-XL over the Debiased AFDB.

Method	PDB	AFDB	Debiased AFDB	Debiased AFDB-XL
StructGNN	32.62	26.04	$29.99_{(+3.95)}$	$30.57_{(+0.58)}$
GraphTrans	32.84	27.05	$30.62_{(+3.57)}$	$30.96_{(+0.34)}$
GVP	34.81	24.35	$31.15_{(+6.80)}$	$31.66_{(+0.51)}$
ProteinMPNN	42.33	26.48	$35.22_{(+8.74)}$	$35.55_{(+0.33)}$
PiFold	43.74	17.74	$35.38_{(+17.64)}$	$35.76_{(+0.38)}$

More detailed experimental analysis and statistics are provided in Appendix D.

7 Conclusion and Limitation

In this work, we identified and addressed a critical challenge in leveraging the vast AFDB for training deep learning models sensitive to precise atomic details, particularly for the task of inverse folding. We demonstrated that a systematic bias exists within AFDB structures. To mitigate this, we propose DeSAE to reconstruct native-like experimental structures from corrupted inputs. Our extensive experiments consistently showed that our debiasing pipeline effectively debiases AFDB without introducing significant global distortions. One limitation of our approach is its focus on backbone geometries, potentially overlooking higher-order structural details such as sidechain orientations.

Acknowledgement

This work was supported by 2025 Local Supporting Project (PJ-PRJ24DATA001) by Shanghai Artificial Intelligence Laboratory, National Science and Technology Major Project (No. 2022ZD0115101), National Natural Science Foundation of China Project (No. 624B2115, No. U21A20427), Project (No. WU2022A009) from the Center of Synthetic Biology and Integrated Bioengineering of Westlake University, Project (No. WU2023C019) from the Westlake University Industries of the Future Research Funding.

References

[1] John Jumper, Richard Evans, Alexander Pritzel, Tim Green, Michael Figurnov, Olaf Ronneberger, Kathryn Tunyasuvunakool, Russ Bates, Augustin Žídek, Anna Potapenko, et al. Highly accurate protein structure prediction with alphafold. *nature*, 596(7873):583–589, 2021.

[2] Richard Evans, Michael O'Neill, Alexander Pritzel, Natasha Antropova, Andrew Senior, Tim Green, Augustin Žídek, Russ Bates, Sam Blackwell, Jason Yim, et al. Protein complex prediction with alphafold-multimer. *biorxiv*, pages 2021–10, 2021.

[3] Josh Abramson, Jonas Adler, Jack Dunger, Richard Evans, Tim Green, Alexander Pritzel, Olaf Ronneberger, Lindsay Willmore, Andrew J Ballard, Joshua Bambrick, et al. Accurate structure prediction of biomolecular interactions with alphafold 3. *Nature*, 630(8016):493–500, 2024.

[4] Mihaly Varadi, Stephen Anyango, Mandar Deshpande, Sreenath Nair, Cindy Natassia, Galabina Yordanova, David Yuan, Oana Stroe, Gemma Wood, Agata Laydon, et al. Alphafold protein structure database: massively expanding the structural coverage of protein-sequence space with high-accuracy models. *Nucleic acids research*, 50(D1):D439–D444, 2022.

[5] Mihaly Varadi, Damian Bertoni, Paulyna Magana, Urmila Paramval, Ivanna Pidruchna, Malarvizhi Radhakrishnan, Maxim Tsenkov, Sreenath Nair, Milot Mirdita, Jingi Yeo, et al. Alphafold protein structure database in 2024: providing structure coverage for over 214 million protein sequences. *Nucleic acids research*, 52(D1):D368–D375, 2024.

[6] Haroldas Bagdonas, Carl A Fogarty, Elisa Fadda, and Jon Agirre. The case for post-predictional modifications in the alphafold protein structure database. *Nature structural & molecular biology*, 28(11):869–870, 2021.

[7] John Ingraham, Vikas Garg, Regina Barzilay, and Tommi Jaakkola. Generative models for graph-based protein design. *Advances in neural information processing systems*, 32, 2019.

[8] Bowen Jing, Stephan Eismann, Patricia Suriana, Raphael John Lamarre Townshend, and Ron Dror. Learning from protein structure with geometric vector perceptrons. In *International Conference on Learning Representations*, 2021.

[9] Zhangyang Gao, Cheng Tan, and Stan Z Li. Pifold: Toward effective and efficient protein inverse folding. In *The Eleventh International Conference on Learning Representations*, 2022.

[10] Chai Discovery. Chai-1: Decoding the molecular interactions of life. *bioRxiv*, 2024.

[11] Jeremy Wohlwend, Gabriele Corso, Saro Passaro, Noah Getz, Mateo Reveiz, Ken Leidal, Wojtek Swiderski, Liam Atkinson, Tally Portnoi, Itamar Chinn, Jacob Silterra, Tommi Jaakkola, and Regina Barzilay. Boltz-1: Democratizing biomolecular interaction modeling. *bioRxiv*, 2024.

[12] Milot Mirdita, Konstantin Schütze, Yoshitaka Moriwaki, Lim Heo, Sergey Ovchinnikov, and Martin Steinegger. Colabfold: making protein folding accessible to all. *Nature methods*, 2022.

[13] Helen M Berman, John Westbrook, Zukang Feng, Gary Gilliland, Talapady N Bhat, Helge Weissig, Ilya N Shindyalov, and Philip E Bourne. The protein data bank. *Nucleic acids research*, 28(1):235–242, 2000.

[14] Kathryn Tunyasuvunakool, Jonas Adler, Zachary Wu, Tim Green, Michal Zielinski, Augustin Žídek, Alex Bridgland, Andrew Cowie, Clemens Meyer, Agata Laydon, et al. Highly accurate protein structure prediction for the human proteome. *Nature*, 596(7873):590–596, 2021.

[15] Jin Su, Chenchen Han, Yuyang Zhou, Junjie Shan, Xibin Zhou, and Fajie Yuan. Saprot: Protein language modeling with structure-aware vocabulary. In *The Twelfth International Conference on Learning Representations*, 2024.

[16] Jin Su, Xibin Zhou, Xuting Zhang, and Fajie Yuan. Protrek: Navigating the protein universe through tri-modal contrastive learning. *bioRxiv*, pages 2024–05, 2024.

[17] Patrick Bryant, Gabriele Pozzati, and Arne Elofsson. Improved prediction of protein-protein interactions using alphafold2. *Nature communications*, 13(1):1265, 2022.

[18] Cheng Tan, Zhangyang Gao, Lirong Wu, Jun Xia, Jiangbin Zheng, Xihong Yang, Yue Liu, Bozhen Hu, and Stan Z Li. Cross-gate mlp with protein complex invariant embedding is a one-shot antibody designer. In *Proceedings of the AAAI Conference on Artificial Intelligence*, volume 38, pages 15222–15230, 2024.

[19] Cheng Tan, Yijie Zhang, Zhangyang Gao, Yufei Huang, Haitao Lin, Lirong Wu, Fandi Wu, Mathieu Blanchette, and Stan Z Li. dyab: Flow matching for flexible antibody design with alphafold-driven pre-binding antigen. In *Proceedings of the AAAI Conference on Artificial Intelligence*, volume 39, pages 782–790, 2025.

[20] Zhangyang Gao, Cheng Tan, Jue Wang, Yufei Huang, Lirong Wu, and Stan Z Li. Foldtoken: Learning protein language via vector quantization and beyond. In *Proceedings of the AAAI Conference on Artificial Intelligence*, volume 39, pages 219–227, 2025.

[21] Bowen Jing, Bonnie Berger, and Tommi Jaakkola. Alphafold meets flow matching for generating protein ensembles. In *Forty-first International Conference on Machine Learning*.

[22] Pascal Notin, Nathan Rollins, Yarin Gal, Chris Sander, and Debora Marks. Machine learning for functional protein design. *Nature biotechnology*, 42(2):216–228, 2024.

[23] Alexander E Chu, Tianyu Lu, and Po-Ssu Huang. Sparks of function by de novo protein design. *Nature biotechnology*, 42(2):203–215, 2024.

[24] Shengchao Liu, Yanjing Li, Zhuoxinran Li, Anthony Gitter, Yutao Zhu, Jiarui Lu, Zhao Xu, Weili Nie, Arvind Ramanathan, Chaowei Xiao, et al. A text-guided protein design framework. *Nature Machine Intelligence*, pages 1–12, 2025.

[25] Han Huang, Ziqian Lin, Dongchen He, Liang Hong, and Yu Li. Ribodiffusion: tertiary structure-based rna inverse folding with generative diffusion models. *Bioinformatics*, 40(Supplement_1):i347–i356, 2024.

[26] Brian Kuhlman and David Baker. Native protein sequences are close to optimal for their structures. *Proceedings of the National Academy of Sciences*, 97(19):10383–10388, 2000.

[27] Ivan Anishchenko, Samuel J Pellock, Tamuka M Chidyausiku, Theresa A Ramelot, Sergey Ovchinnikov, Jingzhou Hao, Khushboo Bafna, Christoffer Norn, Alex Kang, Asim K Bera, et al. De novo protein design by deep network hallucination. *Nature*, 600(7889):547–552, 2021.

[28] Namrata Anand, Raphael Eguchi, Irimpan I Mathews, Carla P Perez, Alexander Derry, Russ B Altman, and Po-Ssu Huang. Protein sequence design with a learned potential. *Nature communications*, 13(1):746, 2022.

[29] Tomas Geffner, Kieran Didi, Zuobai Zhang, Danny Reidenbach, Zhonglin Cao, Jason Yim, Mario Geiger, Christian Dallago, Emine Kucukbenli, Arash Vahdat, et al. Proteina: Scaling flow-based protein structure generative models. In *The Thirteenth International Conference on Learning Representations*, 2025.

[30] Hannes Stark, Bowen Jing, Tomas Geffner, Jason Yim, Tommi Jaakkola, Arash Vahdat, and Karsten Kreis. Protcomposer: Compositional protein structure generation with 3d ellipsoids. In *The Thirteenth International Conference on Learning Representations*, 2025.

[31] Bassil I Dahiyat and Stephen L Mayo. De novo protein design: fully automated sequence selection. *Science*, 278(5335):82–87, 1997.

[32] Wouter Boomsma and Jes Frellsen. Spherical convolutions and their application in molecular modelling. *Advances in neural information processing systems*, 30, 2017.

[33] Hanqun Cao, Cheng Tan, Zhangyang Gao, Yilun Xu, Guangyong Chen, Pheng-Ann Heng, and Stan Z Li. A survey on generative diffusion models. *IEEE Transactions on Knowledge and Data Engineering*, 2024.

[34] Yue Cao, Payel Das, Vijil Chenthamarakshan, Pin-Yu Chen, Igor Melnyk, and Yang Shen. Fold2seq: A joint sequence (1d)-fold (3d) embedding-based generative model for protein design. In *International Conference on Machine Learning*, pages 1261–1271. PMLR, 2021.

[35] Zhixiu Li, Yuedong Yang, Eshel Faraggi, Jian Zhan, and Yaoqi Zhou. Direct prediction of profiles of sequences compatible with a protein structure by neural networks with fragment-based local and energy-based nonlocal profiles. *Proteins: Structure, Function, and Bioinformatics*, 82(10):2565–2573, 2014.

[36] James O'Connell, Zhixiu Li, Jack Hanson, Rhys Heffernan, James Lyons, Kuldip Paliwal, Abdollah Dehzangi, Yuedong Yang, and Yaoqi Zhou. Spin2: Predicting sequence profiles from protein structures using deep neural networks. *Proteins: Structure, Function, and Bioinformatics*, 86(6):629–633, 2018.

[37] Jingxue Wang, Huali Cao, John ZH Zhang, and Yifei Qi. Computational protein design with deep learning neural networks. *Scientific reports*, 8(1):1–9, 2018.

[38] Sheng Chen, Zhe Sun, Lihua Lin, Zifeng Liu, Xun Liu, Yutian Chong, Yutong Lu, Huiying Zhao, and Yuedong Yang. To improve protein sequence profile prediction through image captioning on pairwise residue distance map. *Journal of chemical information and modeling*, 60(1):391–399, 2019.

[39] Yifei Qi and John ZH Zhang. Densecpd: improving the accuracy of neural-network-based computational protein sequence design with densenet. *Journal of chemical information and modeling*, 60(3):1245–1252, 2020.

[40] Yuan Zhang, Yang Chen, Chenran Wang, Chun-Chao Lo, Xiuwen Liu, Wei Wu, and Jinfeng Zhang. Prodconn: Protein design using a convolutional neural network. *Proteins: Structure, Function, and Bioinformatics*, 88(7):819–829, 2020.

[41] Gao Huang, Zhuang Liu, Laurens Van Der Maaten, and Kilian Q Weinberger. Densely connected convolutional networks. In *Proceedings of the IEEE conference on computer vision and pattern recognition*, pages 4700–4708, 2017.

[42] Kai Yi, Bingxin Zhou, Yiqing Shen, Pietro Liò, and Yuguang Wang. Graph denoising diffusion for inverse protein folding. *Advances in Neural Information Processing Systems*, 36:10238–10257, 2023.

[43] Yiheng Zhu, Jialu Wu, Qiuyi Li, Jiahuan Yan, Mingze Yin, Wei Wu, Mingyang Li, Jieping Ye, Zheng Wang, and Jian Wu. Bridge-if: Learning inverse protein folding with markov bridges. In *The Thirty-eighth Annual Conference on Neural Information Processing Systems*, 2024.

[44] Zhangyang Gao, Daize Dong, Cheng Tan, Jun Xia, Bozhen Hu, and Stan Z Li. A graph is worth k words: Euclideanizing graph using pure transformer. In *International Conference on Machine Learning*, pages 14681–14701. PMLR, 2024.

[45] Cheng Tan, Zhangyang Gao, Jun Xia, Bozhen Hu, and Stan Z Li. Global-context aware generative protein design. In *ICASSP 2023-2023 IEEE International Conference on Acoustics, Speech and Signal Processing (ICASSP)*, pages 1–5. IEEE, 2023.

[46] Alexey Strokach, David Becerra, Carles Corbi-Verge, Albert Perez-Riba, and Philip M Kim. Fast and flexible protein design using deep graph neural networks. *Cell Systems*, 11(4):402–411, 2020.

[47] Zhangyang Gao, Cheng Tan, Stan Li, et al. Alphadesign: A graph protein design method and benchmark on alphafolddb. *arXiv preprint arXiv:2202.01079*, 2022.

[48] Justas Dauparas, Ivan Anishchenko, Nathaniel Bennett, Hua Bai, Robert J Ragotte, Lukas F Milles, Basile IM Wicky, Alexis Courbet, Rob J de Haas, Neville Bethel, et al. Robust deep learning–based protein sequence design using proteinmpnn. *Science*, 378(6615):49–56, 2022.

[49] Chloe Hsu, Robert Verkuil, Jason Liu, Zeming Lin, Brian Hie, Tom Sercu, Adam Lerer, and Alexander Rives. Learning inverse folding from millions of predicted structures. In *International conference on machine learning*, pages 8946–8970. PMLR, 2022.

[50] Weian Mao, Muzhi Zhu, Zheng Sun, Shuaike Shen, Lin Yuanbo Wu, Hao Chen, and Chunhua Shen. De novo protein design using geometric vector field networks. In *The Twelfth International Conference on Learning Representations*, 2024.

[51] Xiaoran Jiao, Weian Mao, Wengong Jin, Peiyuan Yang, Hao Chen, and Chunhua Shen. Boltzmann-aligned inverse folding model as a predictor of mutational effects on protein-protein interactions. In *The Thirteenth International Conference on Learning Representations*, 2025.

[52] Zaixiang Zheng, Yifan Deng, Dongyu Xue, Yi Zhou, Fei Ye, and Quanquan Gu. Structure-informed language models are protein designers. In *International conference on machine learning*, pages 42317–42338. PMLR, 2023.

[53] Zhangyang Gao, Cheng Tan, Xingran Chen, Yijie Zhang, Jun Xia, Siyuan Li, and Stan Z Li. Kw-design: Pushing the limit of protein design via knowledge refinement. In *The Twelfth International Conference on Learning Representations*, 2024.

[54] Xinyou Wang, Zaixiang Zheng, Fei Ye, Dongyu Xue, Shujian Huang, and Quanquan Gu. Diffusion language models are versatile protein learners. In *International Conference on Machine Learning*, pages 52309–52333. PMLR, 2024.

[55] Xinyou Wang, Zaixiang Zheng, YE Fei, Dongyu Xue, Shujian Huang, and Quanquan Gu. Dplm-2: A multimodal diffusion protein language model. In *The Thirteenth International Conference on Learning Representations*, 2025.

[56] Zhenqiao Song, Tinglin Huang, Lei Li, and Wengong Jin. Surfpro: Functional protein design based on continuous surface. In *International Conference on Machine Learning*, pages 46074–46088. PMLR, 2024.

[57] Xiangru Tang, Xinwu Ye, Fang Wu, Daniel Shao, Yin Fang, Siming Chen, Dong Xu, and Mark Gerstein. Bc-design: A biochemistry-aware framework for highly accurate inverse protein folding. *bioRxiv*, pages 2024–10, 2024.

[58] Hannes Stärk, Octavian Ganea, Lagnajit Pattanaik, Regina Barzilay, and Tommi Jaakkola. Equibind: Geometric deep learning for drug binding structure prediction. In *International conference on machine learning*, pages 20503–20521. PMLR, 2022.

[59] Gabriele Corso, Hannes Stärk, Bowen Jing, Regina Barzilay, and Tommi S Jaakkola. Diffdock: Diffusion steps, twists, and turns for molecular docking. In *The Eleventh International Conference on Learning Representations*, 2022.

[60] Shitong Luo, Yufeng Su, Xingang Peng, Sheng Wang, Jian Peng, and Jianzhu Ma. Antigen-specific antibody design and optimization with diffusion-based generative models for protein structures. *Advances in Neural Information Processing Systems*, 35:9754–9767, 2022.

[61] Xiangzhe Kong, Wenbing Huang, and Yang Liu. Conditional antibody design as 3d equivariant graph translation. In *The Eleventh International Conference on Learning Representations*, 2023.

[62] Xiangzhe Kong, Wenbing Huang, and Yang Liu. End-to-end full-atom antibody design. In *International Conference on Machine Learning*, pages 17409–17429. PMLR, 2023.

[63] Rishal Aggarwal, Akash Gupta, Vineeth Chelur, CV Jawahar, and U Deva Priyakumar. Deeppocket: ligand binding site detection and segmentation using 3d convolutional neural networks. *Journal of Chemical Information and Modeling*, 62(21):5069–5079, 2021.

[64] Yuyan Ni, Shikun Feng, Xin Hong, Yuancheng Sun, Wei-Ying Ma, Zhi-Ming Ma, Qiwei Ye, and Yanyan Lan. Pre-training with fractional denoising to enhance molecular property prediction. *Nature Machine Intelligence*, 6(10):1169–1178, 2024.

[65] Yi Liu, Limei Wang, Meng Liu, Yuchao Lin, Xuan Zhang, Bora Oztekin, and Shuiwang Ji. Spherical message passing for 3d molecular graphs. In *International Conference on Learning Representations (ICLR)*, 2022.

[66] Minghao Xu, Xinyu Yuan, Santiago Miret, and Jian Tang. Protst: Multi-modality learning of protein sequences and biomedical texts. In *International Conference on Machine Learning*, pages 38749–38767. PMLR, 2023.

[67] Yu Li, Sheng Wang, Ramzan Umarov, Bingqing Xie, Ming Fan, Lihua Li, and Xin Gao. Deepre: sequence-based enzyme ec number prediction by deep learning. *Bioinformatics*, 34(5):760–769, 2018.

[68] Pascal Notin, Aaron Kollasch, Daniel Ritter, Lood Van Niekerk, Steffanie Paul, Han Spinner, Nathan Rollins, Ada Shaw, Rose Orenbuch, Ruben Weitzman, et al. Proteingym: Large-scale benchmarks for protein fitness prediction and design. *Advances in Neural Information Processing Systems*, 36:64331–64379, 2023.

[69] Chenqing Hua, Bozitao Zhong, Sitao Luan, Liang Hong, Guy Wolf, Doina Precup, and Shuangjia Zheng. Reactzyme: A benchmark for enzyme-reaction prediction. *Advances in Neural Information Processing Systems*, 37:26415–26442, 2024.

[70] Hehe Fan, Zhangyang Wang, Yi Yang, and Mohan Kankanhalli. Continuous-discrete convolution for geometry-sequence modeling in proteins. In *The Eleventh International Conference on Learning Representations*, 2022.

[71] Shengchao Liu, Yanjing Li, Zhuoxinran Li, Zhiling Zheng, Chenru Duan, Zhi-Ming Ma, Omar Yaghi, Animashree Anandkumar, Christian Borgs, Jennifer Chayes, et al. Symmetry-informed geometric representation for molecules, proteins, and crystalline materials. *Advances in neural information processing systems*, 36:66084–66101, 2023.

[72] Limei Wang, Haoran Liu, Yi Liu, Jerry Kurtin, and Shuiwang Ji. Learning hierarchical protein representations via complete 3d graph networks. In *The Eleventh International Conference on Learning Representations*, 2023.

[73] Pablo Gainza, Sarah Wehrle, Alexandra Van Hall-Beauvais, Anthony Marchand, Andreas Scheck, Zander Harteveld, Stephen Buckley, Dongchun Ni, Shuguang Tan, Freyr Sverrisson, et al. De novo design of protein interactions with learned surface fingerprints. *Nature*, 617(7959):176–184, 2023.

[74] Peter Mørch Groth, Mads Kerrn, Lars Olsen, Jesper Salomon, and Wouter Boomsma. Kermut: Composite kernel regression for protein variant effects. *Advances in Neural Information Processing Systems*, 37:29514–29565, 2024.

[75] Lirong Wu, Haitao Lin, Yufei Huang, Zhangyang Gao, Cheng Tan, Yunfan Liu, Tailin Wu, and Stan Z Li. Relation-aware equivariant graph networks for epitope-unknown antibody design and specificity optimization. In *Proceedings of the AAAI Conference on Artificial Intelligence*, volume 39, pages 895–904, 2025.

[76] Cheng Tan, Zhenxiao Cao, Zhangyang Gao, Lirong Wu, Siyuan Li, Yufei Huang, Jun Xia, Bozhen Hu, and Stan Z Li. Metoken: Uniform micro-environment token boosts post-translational modification prediction. In *The Thirteenth International Conference on Learning Representations*, 2025.

[77] Jingjie Zhang, Hanqun CAO, Zijun Gao, Xiaorui Wang, and Chunbin Gu. SAGEPhos: Sage bio-coupled and augmented fusion for phosphorylation site detection. In *The Thirteenth International Conference on Learning Representations*, 2025.

[78] Christine A Orengo, Alex D Michie, Susan Jones, David T Jones, Mark B Swindells, and Janet M Thornton. Cath–a hierarchic classification of protein domain structures. *Structure*, 5(8):1093–1109, 1997.

[79] John B Ingraham, Max Baranov, Zak Costello, Karl W Barber, Wujie Wang, Ahmed Ismail, Vincent Frappier, Dana M Lord, Christopher Ng-Thow-Hing, Erik R Van Vlack, et al. Illuminating protein space with a programmable generative model. *Nature*, 623(7989):1070–1078, 2023.

[80] Martin Steinegger and Johannes Söding. Mmseqs2 enables sensitive protein sequence searching for the analysis of massive data sets. *Nature biotechnology*, 35(11):1026–1028, 2017.

[81] Felix Kallenborn, Alejandro Chacon, Christian Hundt, Hassan Sirelkhatim, Kieran Didi, Sooyoung Cha, Christian Dallago, Milot Mirdita, Bertil Schmidt, and Martin Steinegger. Gpu-accelerated homology search with mmseqs2. *bioRxiv*, pages 2024–11, 2024.

A Technical Details

A.1 Structure Consistency Loss

Inspired by Chroma [79], we supervise our model with five complementary loss terms:

$$\mathcal{L} = \mathcal{L}_{global} + \mathcal{L}_{fragment} + \mathcal{L}_{pair} + \mathcal{L}_{neighbor} + \mathcal{L}_{distance} \tag{12}$$

To define these terms, let $X \in \mathbb{R}^{n\times 3}$ be the ground-truth backbone coordinates of n residues and $\hat{X} \in \mathbb{R}^{n\times 3}$ their predictions. We first introduce the basic aligned RMSD loss:

$$\mathcal{L}_{aligned}(\hat{X}, X) = \|\text{Align}(\hat{X}, X) - X\| \tag{13}$$

where $\text{Align}(\hat{X}, X)$ rigidly aligns the prediction to the target before measuring deviation. Thus, the five loss terms are defined based on the aligned RMSD loss as follows:

- **Global Loss ($\mathcal{L}_{global}$):** Apply $\mathcal{L}_{aligned}$ to the full backbone of each residue, treating X as $[n, 4, 3]$ (four atoms per residue).
- **Fragment Loss ($\mathcal{L}_{fragment}$):** For earch residue, consider its sequential fragments of $c = 7$ residues centered around each residue; X has shape $[n, c, 4, 3]$.
- **Pair Loss ($\mathcal{L}_{pair}$):** For each of the $K = 30$ nearest-neighbor residue pairs, measure alignment error over c fragments on both residues, i.e. shape $[n, K, c \cdot 2, 4, 3]$.
- **Neighbor Loss ($\mathcal{L}_{neighbor}$):** Compute RMSD over the four backbone atoms of the K nearest neighbors for each residue, with X shaped $[n, K, 4, 3]$.

Finally, the **Distance Loss ($\mathcal{L}_{distance}$)** enforces correct inter-residue distances using an MSE objective:

$$\mathcal{L}_{distance} = \|\text{Dist}(\hat{X}) - \text{Dist}(X)\| \tag{14}$$

where $\text{Dist}(X) \in R^{n\times n}$ is the matrix of pairwise C$_\alpha$-C$_\alpha$ distances derived from the coordinates X.

We compute each of these five losses at every decoder layer and average them over the L layers. Empirically, this multi-scale supervision is crucial to achieve good global structural fidelity.

A.2 Quat2Rot Function

Let $q = (w, x, y, z)$ be the quaternion, then:

$$R(q) = \begin{pmatrix} w^2 + x^2 - y^2 - z^2 & 2(xy - wz) & 2(xz + wy) \\ 2(xy + wz) & w^2 - x^2 + y^2 - z^2 & 2(yz - wx) \\ 2(xz - wy) & 2(yz + wx) & w^2 - x^2 - y^2 + z^2 \end{pmatrix}, \tag{15}$$

Equivalently, each component of the rotation matrix is given by:

$$\begin{aligned} R_{00} &= w^2 + x^2 - y^2 - z^2, \\ R_{01} &= 2\big(x\,y - w\,z\big), \\ R_{02} &= 2\big(x\,z + w\,y\big), \\ R_{10} &= 2\big(x\,y + w\,z\big), \\ R_{11} &= w^2 - x^2 + y^2 - z^2, \\ R_{12} &= 2\big(y\,z - w\,x\big), \\ R_{20} &= 2\big(x\,z - w\,y\big), \\ R_{21} &= 2\big(y\,z + w\,x\big), \\ R_{22} &= w^2 - x^2 - y^2 + z^2. \end{aligned} \tag{16}$$

B Dataset Details

This section details the curation of datasets used for training the DeSAE and for evaluating its efficacy in downstream tasks, particularly inverse folding. Rigorous procedures were implemented to ensure data quality and prevent information leakage between training and test sets.

B.1 DeSAE Training Dataset: Paired AFDB-PDB Structures

The DeSAE model is trained to learn a mapping from potentially biased predicted structures to conformations more representative of experimental observations. To facilitate this, we constructed a dataset of paired protein structures, where each pair consists of:

1. An AlphaFold-predicted structure sourced from the AFDB [4, 1].
2. Its corresponding experimentally determined structure from the PDB [13].

The curation process for this paired dataset involved several steps:

1. Initial Pairing: We identified all PDB entries that have a corresponding prediction available in the AFDB based on UniProt accession numbers.
2. Quality and Consistency Filtering: To ensure a meaningful structural correspondence and high-quality predictions, we applied the following filters:
   - The AlphaFold prediction must exhibit a mean predicted Local Distance Difference Test (pLDDT) score greater than 70. The choice of a pLDDT score > 70 is a widely adopted convention in the field for filtering high-confidence predictions from AlphaFold [14]. By setting the threshold at >70, we ensure that the AFDB structures used in our study are of high quality while maximizing dataset coverage across the proteome.
   - The sequence lengths of the AFDB-predicted structure and the PDB experimental structure must be identical.
3. Residue-Level Matching: By enforcing identical sequence lengths and originating from the same protein, we ensure a direct residue-to-residue mapping between the predicted and experimental structures within each pair.

This curation process yielded a high-quality dataset of **19,392 AFDB-PDB paired structures**.

B.2 Downstream Task Evaluation: Inverse Folding Datasets

To evaluate the impact of DeSAE-debiasing on inverse folding performance, we prepared three distinct structural datasets derived from our curated pairs:

1. PDB Dataset: The experimental structures from the 19,392 PDB entries.
2. AFDB Dataset: The corresponding AlphaFold predictions from the AFDB.
3. Debiased AFDB Dataset: The AFDB structures after being processed by trained DeSAE model.

Inverse folding models are trained and evaluated separately on these three structural datasets to quantify the effect of debiasing.

B.3 Benchmark Test Sets and Data Leakage Prevention

To assess the generalization capabilities of inverse folding models trained on the aforementioned datasets, we utilized several established benchmark test sets: CATH 4.2 [78], TS50, TS500, and CATH 4.3 [78]. To ensure that our benchmark evaluations are not compromised by data leakage from the DeSAE training set or the inverse folding training sets, we implemented a strict sequence similarity filtering protocol. Using MMseqs2 [80, 81], we removed any protein structure from these benchmark test sets if its sequence exhibited more than 90% sequence identity to any sequence present in our comprehensive 19,392-structure paired dataset used for DeSAE training. Following this filtering, our final benchmark test sets comprise: 893 structures from CATH 4.2, 38 from TS50, 382 from TS500, and 1575 from CATH 4.3. Performance on these carefully curated, non-overlapping test sets provides a robust measure of model generalization.

C Experiment Details

Our experimental methodology involves a two-stage process, followed by downstream task evaluation, as illustrated in Figure 9. First, DeSAE is trained using experimental PDB structures. Second, the trained DeSAE is employed to process and debias AFDB structures. Finally, inverse folding models are trained on the original PDB, original AFDB, and the DeSAE-debiased AFDB structures to evaluate the impact of our debiasing approach.

Stage 1: Pretraining DeSAE on PDB. To initialize our debiasing autoencoder, we trained DeSAE exclusively on the PDB portion of our paired dataset. Training spanned 60 epochs with an initial learning rate of 1×10^{-3}, a batch size of 16, and a CosineAnnealingLR scheduler to anneal the learning rate. The SE(3) encoder comprised eight equivariant layers, and the decoder comprised six layers, each with a hidden dimensionality of 128. In each epoch, we randomly corrupted 10% of the residues in every structure to enforce robustness against atomic perturbations.

Stage 2: Generating a Debiased AFDB. After pretraining, we applied the learned DeSAE as a preprocessing step to our AFDB structures. Specifically, we passed the AFDB entries through DeSAE to mitigate systematic biases in the predicted coordinates, producing a "Debiased AFDB" dataset. Together with the original AFDB and PDB sets, this yielded three distinct paired training datasets for downstream evaluation: (1) PDB, (2) AFDB, and (3) Debiased AFDB.

Stage 3: Inverse Folding Evaluation. To assess the impact of debiasing on inverse folding performance, we trained separate inverse-folding models on each of the three datasets. Each model was trained for 50 epochs with a learning rate of 1×10^{-3} and a batch size of 32. The performance of these three differently trained inverse folding models was then compared on the independent benchmark test sets detailed in Appendix B.

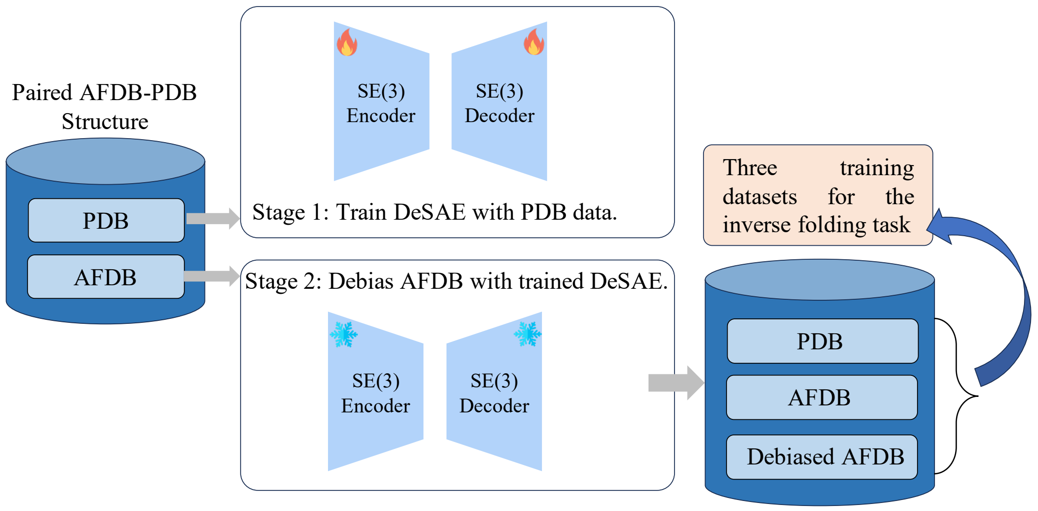
Paired AFDB-PDB Structure
PDB
AFDB
SE(3) Encoder
SE(3) Decoder
Stage 1: Train DeSAE with PDB data.
Stage 2: Debias AFDB with trained DeSAE.
SE(3) Encoder
SE(3) Decoder
Three training datasets for the inverse folding task
PDB
AFDB
Debiased AFDB

Figure 9: Overview of our experimental pipeline. Stage 1 pretrains DeSAE on PDB data; Stage 2 applies DeSAE to AFDB to obtain Debiased AFDB; Stage 3 trains and evaluates inverse-folding models on PDB, AFDB, and Debiased AFDB datasets for comparison.

Baseline To rigorously evaluate our approach, we compare against five state-of-the-art inverse-folding methods: StructGNN [7], GraphTrans [7], GVP [8], ProteinMPNN [48] and PiFold [9]. Each baseline is trained under identical conditions on three distinct datasets: (1) the original AFDB structures, (2) experimentally determined PDB structures, and (3) our debiased AFDB set.
As shown in the main text, models with higher expressive capacity—such as PiFold perform better on PDB dataset, but are dramatically underperformed on AFDB dataset. These models are indeed designed to capture subtle geometric patterns and fine-grained correlations within structural data. When trained on high-fidelity experimental structures from the PDB, these models benefit from the

natural variability and physical realism inherent in the data, leading to strong generalization.

However, AFDB structures, while accurate at the fold level, exhibit systematic geometric regularities due to AlphaFold's inductive biases—such as smoother dihedral angle distributions and reduced local structural noise. High-capacity models can inadvertently latch onto these superficial statistical cues, treating them as meaningful signals. This leads to distribution-specific overfitting: the model internalizes patterns that are predictive only within the synthetic AFDB manifold, rather than learning robust, physically grounded sequence-structure mappings. In contrast, lower-capacity models may act as a natural form of regularization, failing to fully absorb these subtle biases and thus generalizing marginally better.

Metric We primarily employed the sequence recovery rate that measures the residue-wise accuracy:

$$\text{Recovery Rate} = \frac{1}{L}\sum_{i=1}^{L}\mathbb{I}(s_i = s'_i), \tag{17}$$

where $S_{pred} = (s'_1, s'_2, ..., s'_L)$ is the output sequence of inverse folding methods. In addition to recovery rate, we also considered perplexity as a complementary metric. Perplexity is widely used in sequence modeling tasks:

$$\text{Perplexity} = \exp\left(-\frac{1}{L}\sum_{i=1}^{L}\log P(s_i|X)\right) \tag{18}$$

D Additional Experiments

D.1 Evaluating Generalization to AlphaFold Structures

To further investigate the distinct characteristics learned by models trained on different structural data sources, we conducted an auxiliary experiment. In this scenario, we evaluated the performance of inverse folding models trained on PDB, AFDB, and Debiased AFDB structures, **but this time, the test set was constructed using AlphaFold-predicted structures** corresponding to the CATH4.2 benchmark (termed "AFDB-version CATH4.2 test set"). This setup allows us to assess how well models generalize to the specific structural distribution of AlphaFold predictions themselves.

The results, presented in Table 2, reveal several interesting trends. Unsurprisingly, models trained directly on raw AFDB data consistently achieve the highest recovery rates on this AFDB-version test set. This is expected, as the training and testing distributions are perfectly matched, and the models have effectively learned the idiosyncratic features and potential biases inherent in AlphaFold's predictions. Interestingly, models trained on Debiased AFDB structures achieve the second-best performance. While the debiasing process aims to shift AFDB structures towards the PDB distribution, these structures evidently retain sufficient AFDB-like characteristics to perform well when tested on AFDB predictions, outperforming models trained solely on PDB data for most architectures.

Notably, models trained exclusively on experimental PDB structures, despite having no exposure to AlphaFold's specific predictive patterns or biases during training, still demonstrate commendable generalization to the AFDB-version test set. For instance, PiFold trained on PDB achieves a recovery rate of 44.31%. This suggests that experimental structures encapsulate fundamental sequence-structure relationships that possess inherent generalizability, even to predicted structures that might deviate subtly from experimental reality. This observation reinforces the concept that PDB structures, while potentially "noisier," represent a more foundational and broadly applicable structural truth. The strong performance of AFDB-trained models on AFDB test data further underscores the existence of a distinct "AFDB manifold" which models can readily learn, but which may not perfectly align with the manifold of experimental structures.

D.2 Differential Impact of Large-Scale DeSAE Pretraining on Recovery and Perplexity

Our previous analysis in Table 1 indicated that pretraining DeSAE on an expanded PDB dataset provided Debiased AFDB-XL which yielded only marginal improvements in the sequence recovery

Table 2: Recovery rate (%) of inverse folding methods trained different data and test on the AFDB-version CATH4.2 test set.

Method	PDB	AFDB	Debiased AFDB
StructGNN	34.21	37.83	36.16
GraphTrans	33.74	43.45	36.64
GVP	35.60	45.22	37.63
ProteinMPNN	41.87	76.83	45.34
PiFold	44.31	62.87	46.35

rate. To gain a more nuanced understanding of the effects of this larger-scale pretraining, we further evaluated the models using the perplexity metric, where lower values signify better performance by indicating higher confidence in the predicted amino acid probabilities.

The results, presented in Table 3, reveal a more pronounced benefit of using Debiased AFDB-XL when assessed by perplexity. Across all inverse folding architectures tested on the CATH 4.3 set, models trained on Debiased AFDB-XL consistently achieved lower (i.e., better) perplexity scores compared to those trained on the standard Debiased AFDB. This divergence suggests that while the additional structural information learned by DSAE-XL from the larger PDB corpus may not substantially alter the single best amino acid prediction at each position (thus leading to minor changes in recovery rate), it does refine the overall probability distribution over possible amino acids. The model becomes more confident in its correct predictions and less confident in incorrect ones, leading to lower perplexity.

Table 3: Perpelxity metric of inverse folding methods trained on different data and test on the CATH 4.3 test set.

Method	PDB	AFDB	Debiased AFDB	Debiased AFDB-XL
StructGNN	8.81	11.90	10.64	9.67
GraphTrans	8.75	14.09	10.55	9.56
GVP	8.07	16.59	10.14	9.25
ProteinMPNN	7.07	11.70	10.19	8.77
PiFold	6.42	13.83	10.39	8.43

D.3 Experimental sensitivity to the mask ratio

In the training stage of DeSAE, we specified the mask ratio to 0.1. However, we did not elaborate here on the rationale behind selecting this parameter or on the sensitivity of downstream tasks to it. To empirically validate the robustness of our approach, we conducted an ablation study to assess how performance changes with different corruption rates. We trained DeSAE using rates of 10%, 20%, and 30% and then evaluated the performance of downstream inverse folding models trained on the resulting debiased datasets.

Table 4: Performance under different mask ratios. Values in parentheses indicate change relative to mask=10%.

Model	Mask=10%	Mask=20%	Mask=30%
StructGNN	30.50	30.45 (-0.05)	32.06 (+1.56)
GraphTrans	31.29	32.53 (+1.24)	32.68 (+1.39)
GVP	31.44	34.27 (+2.83)	34.14 (+2.70)
ProteinMPNN	36.46	38.64 (+2.18)	38.55 (+2.09)
PiFold	35.68	35.66 (-0.02)	38.41 (+2.73)

As result shown in 4, the results clearly demonstrate that the performance is not critically sensitive to the 10% rate. For most models, performance is stable or even improves with higher corruption rates. This indicates that our method is robust and that forcing the model to solve a more challenging reconstruction task may lead it to learn an even more generalizable representation of the structural manifold. The 10% rate used in the paper is a conservative but effective choice, and the method's strong performance across a range of rates confirms its stability.

E Structure Features Analysis

E.1 Quantitive Analysis

Bond length To quantitatively substantiate our hypothesis regarding systematic differences between AFDB and PDB structural ensembles, we performed a detailed statistical analysis of canonical backbone bond lengths: Cα-N, C-Cα, O-C, and N-C. The comparative statistics are summarized in Table 5. While the mean values for these bond lengths are highly comparable between AFDB and PDB structures, their variances differ substantially. Across all four analyzed bond types, PDB structures consistently exhibit significantly larger variances.

Table 5: Comparison of bond length statistics between AFDB and PDB structures.

	Cα-N	C-Cα	O-C	N-C
AFDB	1.4654±3.68×10^{-5}	1.5323±4.11×10^{-5}	1.2305±1.40×10^{-5}	1.3351±2.39×10^{-5}
PDB	1.4610±**16.95**×10^{-5}	1.5248±**15.48**×10^{-5}	1.2336±**14.14**×10^{-5}	1.3308±**9.57**×10^{-5}

This pattern of significantly tighter bond length distributions in AFDB structures suggests a higher degree of geometric regularity and uniformity compared to experimental structures. It implies that AFDB predictions may not fully capture the natural conformational fluctuations and slight deviations present in the PDB, potentially reflecting an "over-regularization" or a confinement to a narrower, more idealized region of the conformational landscape. This quantitative finding lends strong support to our premise that AFDB structures possess distinct statistical properties that can contribute to the observed generalization gap in downstream tasks sensitive to such fine-grained structural details.

Angle distribution To quantitatively assess the geometric differences between predicted and experimental structures, we analyzed the distributions of key backbone angles within our paired dataset, comparing structures from AFDB against their corresponding PDB entries. We focused on the distributions of three backbone dihedral angles (ϕ, ψ, ω) and three backbone bond angles (α, β, γ) defined as follows for residue i:

Dihedral angles:

- ϕ_i, angle defined by atoms C_{i-1}-N_i-$\mathrm{C}\alpha_i$-C_i.
- ψ_i, angle defined by atoms N_i-$\mathrm{C}\alpha_i$-C_i-N_{i+1}.
- ω_i, angle defined by atoms $\mathrm{C}\alpha_i$-C_i-N_{i+1}-$\mathrm{C}\alpha_{i+1}$.

Bond angles:

- α_i, bond angle N_i-$\mathrm{C}\alpha_i$-C_i.
- β_i, bond angle C_{i-1}-N_i-$\mathrm{C}\alpha_i$.
- ω_i, bond angle $\mathrm{C}\alpha_i$-C_i-N_{i+1}.

The distributions of these six angles were computed separately for the AFDB and PDB structure sets. To quantify the divergence between these distributions, we employed several distance and similarity metrics: Kullback-Leibler (KL) divergence, Wasserstein distance (Earth Mover's Distance), Euclidean distance, and Cosine similarity.

Table 6 presents these comparison metrics. The results indicate noticeable differences between the AFDB and PDB angle distributions. For instance, the dihedral angles ψ and ϕ, which define the Ramachandran plot, exhibit relatively larger KL divergences and Euclidean distances, and lower cosine similarities, compared to the bond angles (α, β, γ). This suggests that AFDB predictions, while generally accurate, may possess subtly different conformational preferences or a more restricted sampling of these crucial dihedral spaces compared to the ensemble of experimental structures.

Table 6: Comparison of different dihedral angle distributions using various distance metrics.

	KL ($\times 10^{-7}$)	Wasserstein ($\times 10^{-8}$)	Euclidean Distance	Cosine Similarity
ϕ	1.5663	5.0828	333.0086	0.9764
ψ	3.6680	2.5720	871.7690	0.9349
ω	2.6013	5.2714	355.6580	0.9894
α	0.0057	3.5109	86.5567	0.9950
β	0.0043	2.7487	75.5303	0.9964
γ	0.0012	1.8125	40.1267	0.9991

E.2 Qualitative Analysis

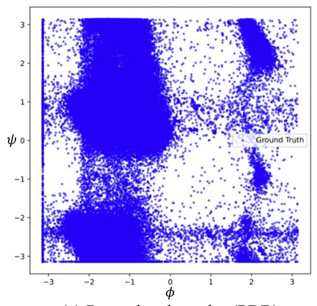

(a) Ramachandran plot (PDB)

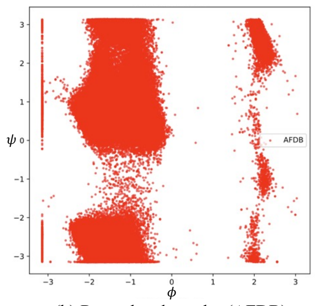

(b) Ramachandran plot (AFDB)

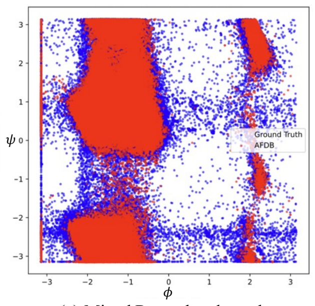

(c) Mixed Ramachandran plot

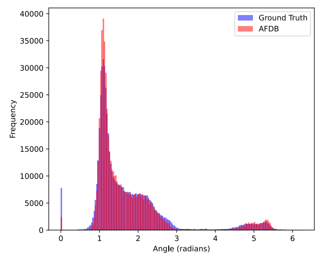

(d) ϕ distribution comparison

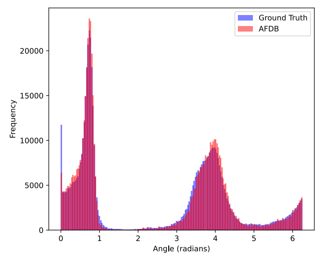

(e) ψ distribution comparison

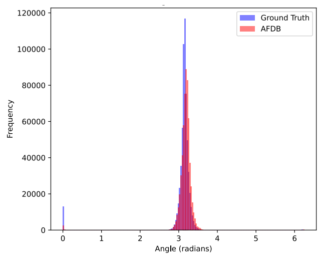

(f) ω distribution comparison

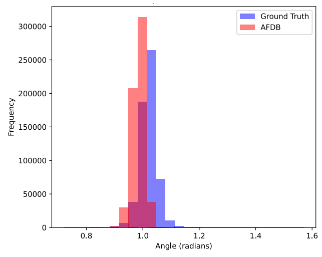

(g) α distribution comparison

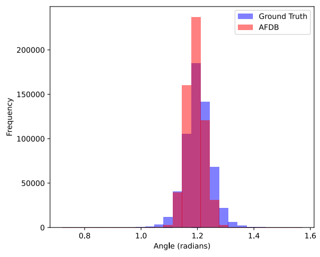

(h) γ distribution comparison

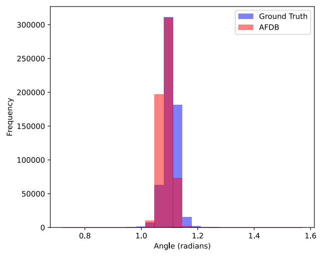

(i) β distribution comparison

Figure 10: Global feature visualization of dihedral angles and bond angles.

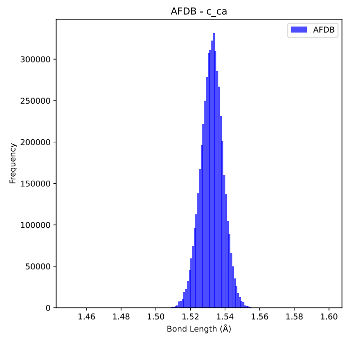

(a) C-Cα distance on AFDB

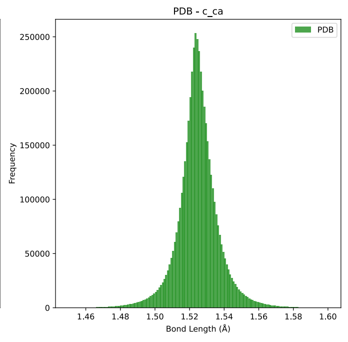

(b) C-Cα distance on PDB

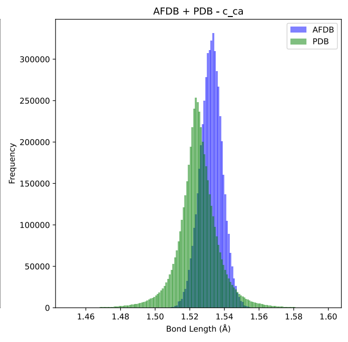

(c) C-Cα distance Comparison

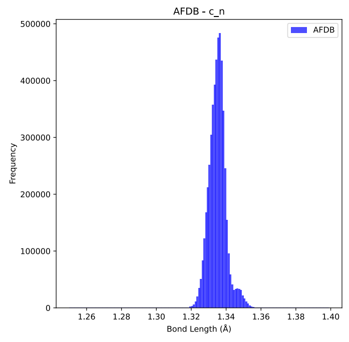

(d) N-C distance on AFDB

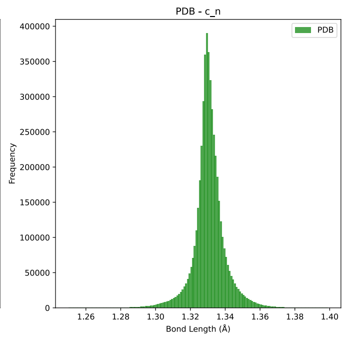

(e) N-C distance on PDB

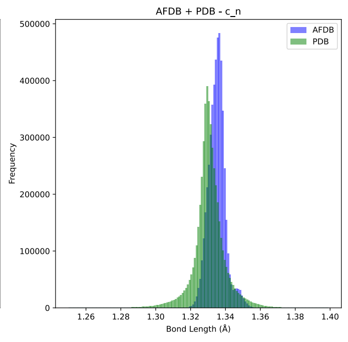

(f) N-C distance Comparison

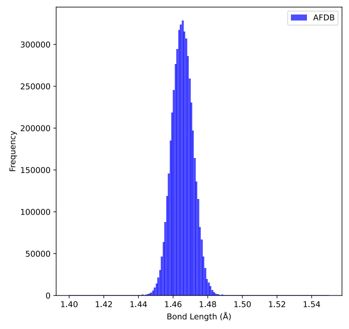

(g) N-Cα distance on AFDB

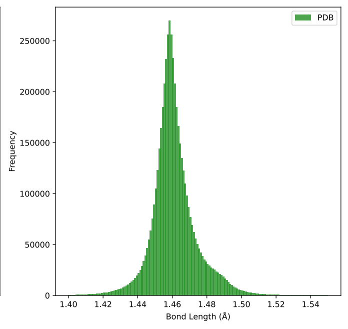

(h) N-Cα distance on PDB

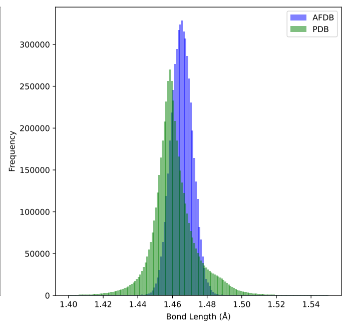

(i) N-Cα distance Comparison

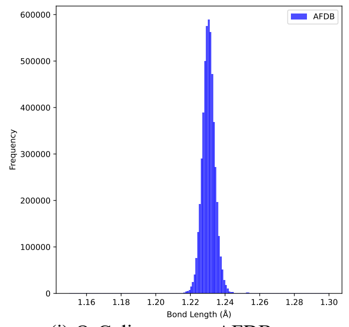

(j) O-C distance on AFDB

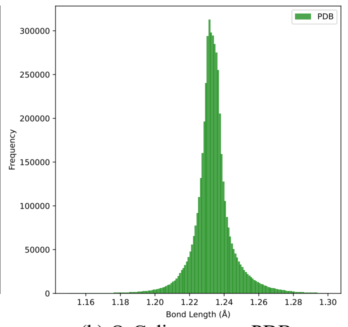

(k) O-C distance on PDB

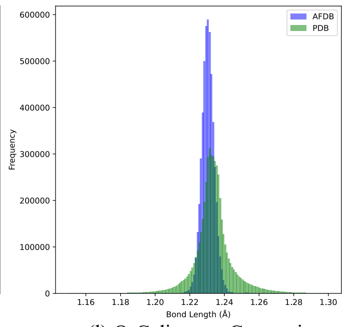

(l) O-C distance Comparison

Figure 11: Bond length visualization.

F Visualization

To provide a qualitative perspective on the structural modifications introduced by our DeSAE, we visualized representative protein structures from PDB, their corresponding AFDB predictions, and the DSAE-processed Debiased AFDB versions. Figure 12 presents several such examples, with structures superimposed for comparison. At a global level, visual inspection reveals that both the raw AFDB predictions and the Debiased AFDB structures maintain high fidelity to the experimental PDB structures, exhibiting similar overall folds and tertiary arrangements.

These visualizations underscore a key aspect of our findings: **the systematic biases in AFDB that impede inverse folding performance are often not readily apparent through casual visual inspection of global structure**. The differences, while quantitatively significant for downstream deep learning models sensitive to local geometric details, can be quite subtle.

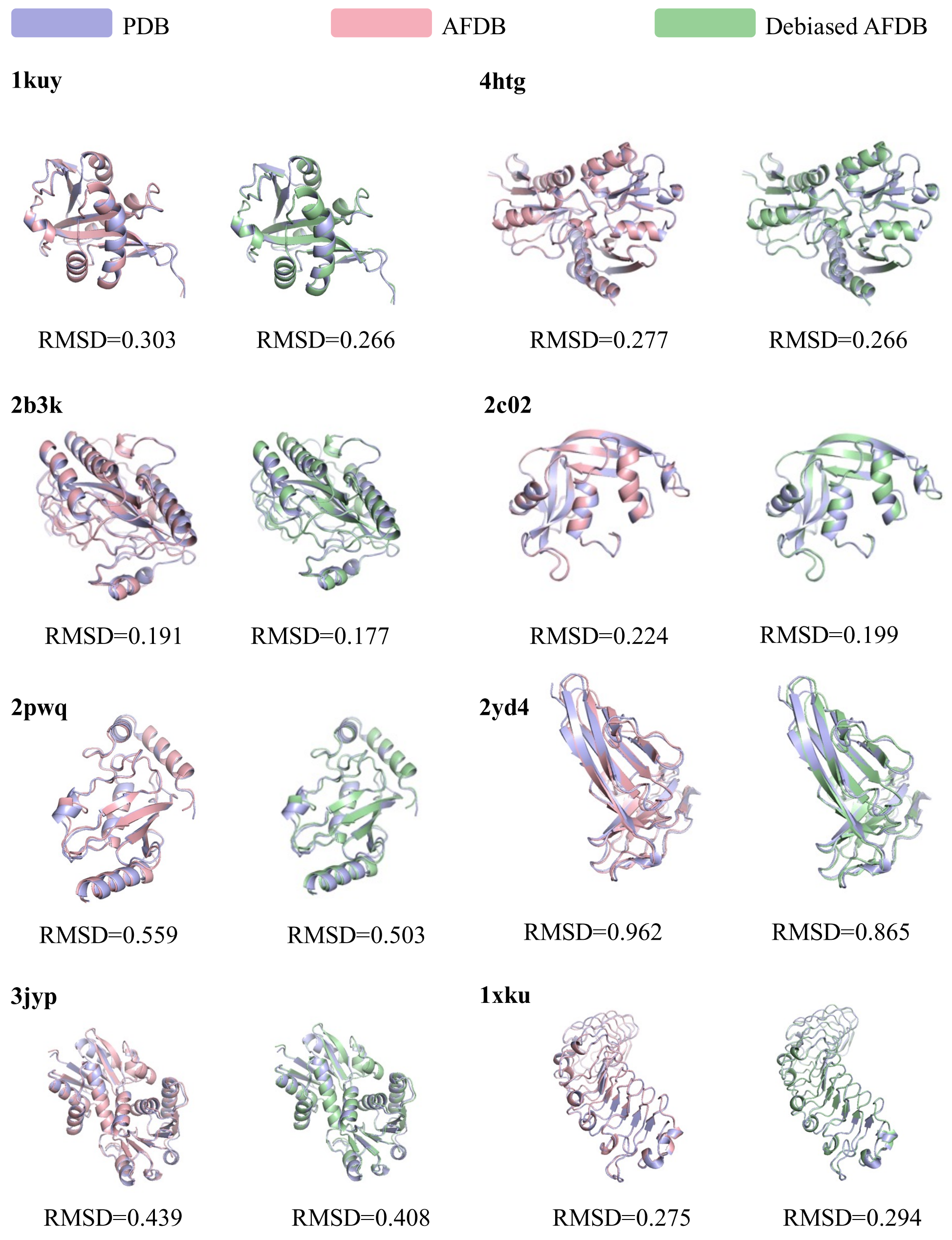

Figure 12: The visualization of samples in PDB, AFDB, and Debiased AFDB.

NeurIPS Paper Checklist

The checklist is designed to encourage best practices for responsible machine learning research, addressing issues of reproducibility, transparency, research ethics, and societal impact. Do not remove the checklist: **The papers not including the checklist will be desk rejected.** The checklist should follow the references and follow the (optional) supplemental material. The checklist does NOT count towards the page limit.

Please read the checklist guidelines carefully for information on how to answer these questions. For each question in the checklist:

- You should answer [Yes] , [No] , or [NA] .
- [NA] means either that the question is Not Applicable for that particular paper or the relevant information is Not Available.
- Please provide a short (1–2 sentence) justification right after your answer (even for NA).

The checklist answers are an integral part of your paper submission. They are visible to the reviewers, area chairs, senior area chairs, and ethics reviewers. You will be asked to also include it (after eventual revisions) with the final version of your paper, and its final version will be published with the paper.

The reviewers of your paper will be asked to use the checklist as one of the factors in their evaluation. While "[Yes] " is generally preferable to "[No] ", it is perfectly acceptable to answer "[No] " provided a proper justification is given (e.g., "error bars are not reported because it would be too computationally expensive" or "we were unable to find the license for the dataset we used"). In general, answering "[No] " or "[NA] " is not grounds for rejection. While the questions are phrased in a binary way, we acknowledge that the true answer is often more nuanced, so please just use your best judgment and write a justification to elaborate. All supporting evidence can appear either in the main paper or the supplemental material, provided in appendix. If you answer [Yes] to a question, in the justification please point to the section(s) where related material for the question can be found.

IMPORTANT, please:

- **Delete this instruction block, but keep the section heading “NeurIPS Paper Checklist"**,
- **Keep the checklist subsection headings, questions/answers and guidelines below.**
- **Do not modify the questions and only use the provided macros for your answers**.

1. **Claims**

   Question: Do the main claims made in the abstract and introduction accurately reflect the paper’s contributions and scope?

   Answer: [Yes]

   Justification: We claimed that the paper addresses the problem of AlphaFold data’s bias.

   Guidelines:

   - The answer NA means that the abstract and introduction do not include the claims made in the paper.
   - The abstract and/or introduction should clearly state the claims made, including the contributions made in the paper and important assumptions and limitations. A No or NA answer to this question will not be perceived well by the reviewers.
   - The claims made should match theoretical and experimental results, and reflect how much the results can be expected to generalize to other settings.
   - It is fine to include aspirational goals as motivation as long as it is clear that these goals are not attained by the paper.

2. **Limitations**

   Question: Does the paper discuss the limitations of the work performed by the authors?

   Answer: [Yes]

   Justification: We have discussed the limitations in the "Conclusion and Limitation" section.

Guidelines:

- The answer NA means that the paper has no limitation while the answer No means that the paper has limitations, but those are not discussed in the paper.
- The authors are encouraged to create a separate "Limitations" section in their paper.
- The paper should point out any strong assumptions and how robust the results are to violations of these assumptions (e.g., independence assumptions, noiseless settings, model well-specification, asymptotic approximations only holding locally). The authors should reflect on how these assumptions might be violated in practice and what the implications would be.
- The authors should reflect on the scope of the claims made, e.g., if the approach was only tested on a few datasets or with a few runs. In general, empirical results often depend on implicit assumptions, which should be articulated.
- The authors should reflect on the factors that influence the performance of the approach. For example, a facial recognition algorithm may perform poorly when image resolution is low or images are taken in low lighting. Or a speech-to-text system might not be used reliably to provide closed captions for online lectures because it fails to handle technical jargon.
- The authors should discuss the computational efficiency of the proposed algorithms and how they scale with dataset size.
- If applicable, the authors should discuss possible limitations of their approach to address problems of privacy and fairness.
- While the authors might fear that complete honesty about limitations might be used by reviewers as grounds for rejection, a worse outcome might be that reviewers discover limitations that aren't acknowledged in the paper. The authors should use their best judgment and recognize that individual actions in favor of transparency play an important role in developing norms that preserve the integrity of the community. Reviewers will be specifically instructed to not penalize honesty concerning limitations.

3. **Theory assumptions and proofs**

   Question: For each theoretical result, does the paper provide the full set of assumptions and a complete (and correct) proof?

   Answer: [NA]

   Justification: There is no complicated theoretical results.

   Guidelines:

   - The answer NA means that the paper does not include theoretical results.
   - All the theorems, formulas, and proofs in the paper should be numbered and cross-referenced.
   - All assumptions should be clearly stated or referenced in the statement of any theorems.
   - The proofs can either appear in the main paper or the supplemental material, but if they appear in the supplemental material, the authors are encouraged to provide a short proof sketch to provide intuition.
   - Inversely, any informal proof provided in the core of the paper should be complemented by formal proofs provided in appendix or supplemental material.
   - Theorems and Lemmas that the proof relies upon should be properly referenced.

4. **Experimental result reproducibility**

   Question: Does the paper fully disclose all the information needed to reproduce the main experimental results of the paper to the extent that it affects the main claims and/or conclusions of the paper (regardless of whether the code and data are provided or not)?

   Answer: [Yes]

   Justification: We have reported the experimental details in the both main text and appendix.

   Guidelines:

   - The answer NA means that the paper does not include experiments.

- If the paper includes experiments, a No answer to this question will not be perceived well by the reviewers: Making the paper reproducible is important, regardless of whether the code and data are provided or not.
- If the contribution is a dataset and/or model, the authors should describe the steps taken to make their results reproducible or verifiable.
- Depending on the contribution, reproducibility can be accomplished in various ways. For example, if the contribution is a novel architecture, describing the architecture fully might suffice, or if the contribution is a specific model and empirical evaluation, it may be necessary to either make it possible for others to replicate the model with the same dataset, or provide access to the model. In general. releasing code and data is often one good way to accomplish this, but reproducibility can also be provided via detailed instructions for how to replicate the results, access to a hosted model (e.g., in the case of a large language model), releasing of a model checkpoint, or other means that are appropriate to the research performed.
- While NeurIPS does not require releasing code, the conference does require all submissions to provide some reasonable avenue for reproducibility, which may depend on the nature of the contribution. For example
  (a) If the contribution is primarily a new algorithm, the paper should make it clear how to reproduce that algorithm.
  (b) If the contribution is primarily a new model architecture, the paper should describe the architecture clearly and fully.
  (c) If the contribution is a new model (e.g., a large language model), then there should either be a way to access this model for reproducing the results or a way to reproduce the model (e.g., with an open-source dataset or instructions for how to construct the dataset).
  (d) We recognize that reproducibility may be tricky in some cases, in which case authors are welcome to describe the particular way they provide for reproducibility. In the case of closed-source models, it may be that access to the model is limited in some way (e.g., to registered users), but it should be possible for other researchers to have some path to reproducing or verifying the results.

5. **Open access to data and code**

   Question: Does the paper provide open access to the data and code, with sufficient instructions to faithfully reproduce the main experimental results, as described in supplemental material?

   Answer: [Yes]

   Justification: We will release the data and code.

   Guidelines:

   - The answer NA means that paper does not include experiments requiring code.
   - Please see the NeurIPS code and data submission guidelines (`https://nips.cc/public/guides/CodeSubmissionPolicy`) for more details.
   - While we encourage the release of code and data, we understand that this might not be possible, so “No” is an acceptable answer. Papers cannot be rejected simply for not including code, unless this is central to the contribution (e.g., for a new open-source benchmark).
   - The instructions should contain the exact command and environment needed to run to reproduce the results. See the NeurIPS code and data submission guidelines (`https://nips.cc/public/guides/CodeSubmissionPolicy`) for more details.
   - The authors should provide instructions on data access and preparation, including how to access the raw data, preprocessed data, intermediate data, and generated data, etc.
   - The authors should provide scripts to reproduce all experimental results for the new proposed method and baselines. If only a subset of experiments are reproducible, they should state which ones are omitted from the script and why.
   - At submission time, to preserve anonymity, the authors should release anonymized versions (if applicable).

- Providing as much information as possible in supplemental material (appended to the paper) is recommended, but including URLs to data and code is permitted.

6. **Experimental setting/details**

   Question: Does the paper specify all the training and test details (e.g., data splits, hyper-parameters, how they were chosen, type of optimizer, etc.) necessary to understand the results?

   Answer: [Yes]

   Justification: We have reported the experimental details in the both main text and appendix.

   Guidelines:

   - The answer NA means that the paper does not include experiments.
   - The experimental setting should be presented in the core of the paper to a level of detail that is necessary to appreciate the results and make sense of them.
   - The full details can be provided either with the code, in appendix, or as supplemental material.

7. **Experiment statistical significance**

   Question: Does the paper report error bars suitably and correctly defined or other appropriate information about the statistical significance of the experiments?

   Answer: [NA]

   Justification: We follow the previous works that do not include error bars.

   Guidelines:

   - The answer NA means that the paper does not include experiments.
   - The authors should answer "Yes" if the results are accompanied by error bars, confidence intervals, or statistical significance tests, at least for the experiments that support the main claims of the paper.
   - The factors of variability that the error bars are capturing should be clearly stated (for example, train/test split, initialization, random drawing of some parameter, or overall run with given experimental conditions).
   - The method for calculating the error bars should be explained (closed form formula, call to a library function, bootstrap, etc.)
   - The assumptions made should be given (e.g., Normally distributed errors).
   - It should be clear whether the error bar is the standard deviation or the standard error of the mean.
   - It is OK to report 1-sigma error bars, but one should state it. The authors should preferably report a 2-sigma error bar than state that they have a 96% CI, if the hypothesis of Normality of errors is not verified.
   - For asymmetric distributions, the authors should be careful not to show in tables or figures symmetric error bars that would yield results that are out of range (e.g. negative error rates).
   - If error bars are reported in tables or plots, The authors should explain in the text how they were calculated and reference the corresponding figures or tables in the text.

8. **Experiments compute resources**

   Question: For each experiment, does the paper provide sufficient information on the computer resources (type of compute workers, memory, time of execution) needed to reproduce the experiments?

   Answer: [Yes]

   Justification: All the experiments are conducted on a single NVIDIA A100 GPU.

   Guidelines:

   - The answer NA means that the paper does not include experiments.
   - The paper should indicate the type of compute workers CPU or GPU, internal cluster, or cloud provider, including relevant memory and storage.

- The paper should provide the amount of compute required for each of the individual experimental runs as well as estimate the total compute.
- The paper should disclose whether the full research project required more compute than the experiments reported in the paper (e.g., preliminary or failed experiments that didn't make it into the paper).

9. **Code of ethics**

   Question: Does the research conducted in the paper conform, in every respect, with the NeurIPS Code of Ethics `https://neurips.cc/public/EthicsGuidelines`?

   Answer: [Yes]

   Justification: We have reviewed the NeurIPS Code of Ethics.

   Guidelines:

   - The answer NA means that the authors have not reviewed the NeurIPS Code of Ethics.
   - If the authors answer No, they should explain the special circumstances that require a deviation from the Code of Ethics.
   - The authors should make sure to preserve anonymity (e.g., if there is a special consideration due to laws or regulations in their jurisdiction).

10. **Broader impacts**

    Question: Does the paper discuss both potential positive societal impacts and negative societal impacts of the work performed?

    Answer: [NA]

    Justification: This paper focuses on fundamental scientific problem that may not have direct societal impacts.

    Guidelines:

    - The answer NA means that there is no societal impact of the work performed.
    - If the authors answer NA or No, they should explain why their work has no societal impact or why the paper does not address societal impact.
    - Examples of negative societal impacts include potential malicious or unintended uses (e.g., disinformation, generating fake profiles, surveillance), fairness considerations (e.g., deployment of technologies that could make decisions that unfairly impact specific groups), privacy considerations, and security considerations.
    - The conference expects that many papers will be foundational research and not tied to particular applications, let alone deployments. However, if there is a direct path to any negative applications, the authors should point it out. For example, it is legitimate to point out that an improvement in the quality of generative models could be used to generate deepfakes for disinformation. On the other hand, it is not needed to point out that a generic algorithm for optimizing neural networks could enable people to train models that generate Deepfakes faster.
    - The authors should consider possible harms that could arise when the technology is being used as intended and functioning correctly, harms that could arise when the technology is being used as intended but gives incorrect results, and harms following from (intentional or unintentional) misuse of the technology.
    - If there are negative societal impacts, the authors could also discuss possible mitigation strategies (e.g., gated release of models, providing defenses in addition to attacks, mechanisms for monitoring misuse, mechanisms to monitor how a system learns from feedback over time, improving the efficiency and accessibility of ML).

11. **Safeguards**

    Question: Does the paper describe safeguards that have been put in place for responsible release of data or models that have a high risk for misuse (e.g., pretrained language models, image generators, or scraped datasets)?

    Answer: [NA]

    Justification: There is no potential risk for misuse.

    Guidelines:

- The answer NA means that the paper poses no such risks.
- Released models that have a high risk for misuse or dual-use should be released with necessary safeguards to allow for controlled use of the model, for example by requiring that users adhere to usage guidelines or restrictions to access the model or implementing safety filters.
- Datasets that have been scraped from the Internet could pose safety risks. The authors should describe how they avoided releasing unsafe images.
- We recognize that providing effective safeguards is challenging, and many papers do not require this, but we encourage authors to take this into account and make a best faith effort.

12. **Licenses for existing assets**

    Question: Are the creators or original owners of assets (e.g., code, data, models), used in the paper, properly credited and are the license and terms of use explicitly mentioned and properly respected?

    Answer: [Yes]

    Justification: We have cited the original owners of the data.

    Guidelines:

    - The answer NA means that the paper does not use existing assets.
    - The authors should cite the original paper that produced the code package or dataset.
    - The authors should state which version of the asset is used and, if possible, include a URL.
    - The name of the license (e.g., CC-BY 4.0) should be included for each asset.
    - For scraped data from a particular source (e.g., website), the copyright and terms of service of that source should be provided.
    - If assets are released, the license, copyright information, and terms of use in the package should be provided. For popular datasets, `paperswithcode.com/datasets` has curated licenses for some datasets. Their licensing guide can help determine the license of a dataset.
    - For existing datasets that are re-packaged, both the original license and the license of the derived asset (if it has changed) should be provided.
    - If this information is not available online, the authors are encouraged to reach out to the asset's creators.

13. **New assets**

    Question: Are new assets introduced in the paper well documented and is the documentation provided alongside the assets?

    Answer: [NA]

    Justification: No new assets.

    Guidelines:

    - The answer NA means that the paper does not release new assets.
    - Researchers should communicate the details of the dataset/code/model as part of their submissions via structured templates. This includes details about training, license, limitations, etc.
    - The paper should discuss whether and how consent was obtained from people whose asset is used.
    - At submission time, remember to anonymize your assets (if applicable). You can either create an anonymized URL or include an anonymized zip file.

14. **Crowdsourcing and research with human subjects**

    Question: For crowdsourcing experiments and research with human subjects, does the paper include the full text of instructions given to participants and screenshots, if applicable, as well as details about compensation (if any)?

    Answer: [NA]

Justification: No such experiments.

Guidelines:

- The answer NA means that the paper does not involve crowdsourcing nor research with human subjects.
- Including this information in the supplemental material is fine, but if the main contribution of the paper involves human subjects, then as much detail as possible should be included in the main paper.
- According to the NeurIPS Code of Ethics, workers involved in data collection, curation, or other labor should be paid at least the minimum wage in the country of the data collector.

15. **Institutional review board (IRB) approvals or equivalent for research with human subjects**

    Question: Does the paper describe potential risks incurred by study participants, whether such risks were disclosed to the subjects, and whether Institutional Review Board (IRB) approvals (or an equivalent approval/review based on the requirements of your country or institution) were obtained?

    Answer: [NA]

    Justification: This paper does not involve crowdsourcing nor research with human subjects.

    Guidelines:

    - The answer NA means that the paper does not involve crowdsourcing nor research with human subjects.
    - Depending on the country in which research is conducted, IRB approval (or equivalent) may be required for any human subjects research. If you obtained IRB approval, you should clearly state this in the paper.
    - We recognize that the procedures for this may vary significantly between institutions and locations, and we expect authors to adhere to the NeurIPS Code of Ethics and the guidelines for their institution.
    - For initial submissions, do not include any information that would break anonymity (if applicable), such as the institution conducting the review.

16. **Declaration of LLM usage**

    Question: Does the paper describe the usage of LLMs if it is an important, original, or non-standard component of the core methods in this research? Note that if the LLM is used only for writing, editing, or formatting purposes and does not impact the core methodology, scientific rigorousness, or originality of the research, declaration is not required.

    Answer: [Yes]

    Justification: We only use LLM for writing and editing.

    Guidelines:

    - The answer NA means that the core method development in this research does not involve LLMs as any important, original, or non-standard components.
    - Please refer to our LLM policy (`https://neurips.cc/Conferences/2025/LLM`) for what should or should not be described.